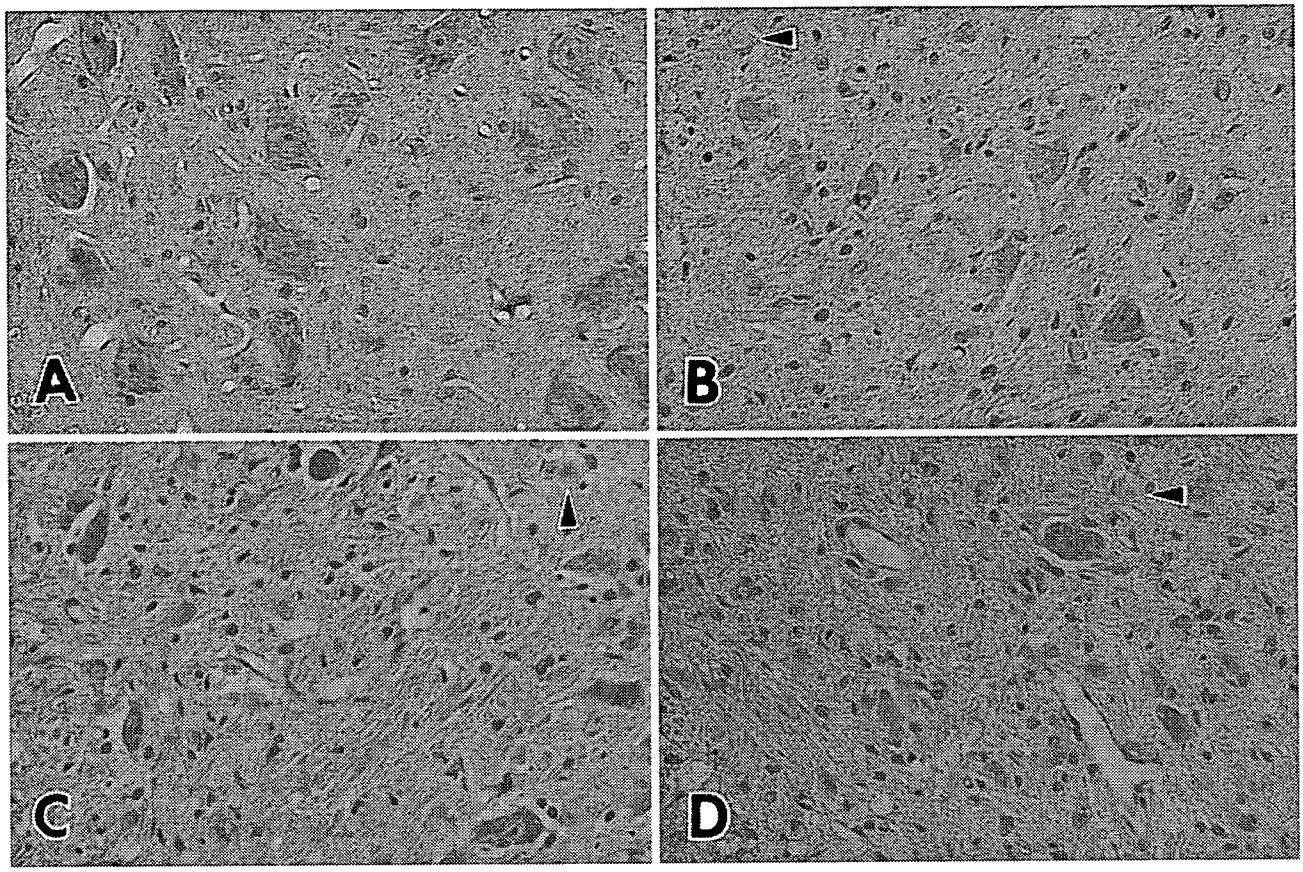

Fig. 3 Histological and histopathological findings in H46R transgenic rats and littermate. (A) The anterior horn of the spinal cord in littermate rat at the age of 160 days: approximately 15 normal anterior horn cells can be observed. (B) The anterior horn of the spinal cord in H46R transgenic rat at the age of 160 days: approximately six anterior horn cells can be counted in the H46R transgenic rat of this age, that is, the number of the anterior horn cells is decreased with astrocytic gliosis, histopathologically, in comparison with the littermate at the same age in (A). A core and halo-type astrocytic hyaline inclusion (Ast-HI) is evident (arrowhead). (C) The anterior horn of the spinal cord in the H46R transgenic rat at the age of 170 days: the histopathological finding of this age reveals loss of the anterior horn cells and gliosis of the spinal cords. A core and halo-type Ast-HI can be observed (arrowhead). (D) The anterior horn of the spinal cord in the H46R transgenic rat at the age of 200 days corresponding to the end-stage: approximately two anterior horn cells can be recognized at this terminal stage; the H46R rats of the terminal stage show severe loss of the anterior horn cells with gliosis of the spinal cords histopathologically compatible with those in ALS patients with clinical courses of over 5 years. A core and halo-type Ast-HI can be seen (arrowhead). As in human ALS patients, small-sized remaining anterior horn cells that appear to be normal are also observed throughout the disease courses in H46R transgenic rats (B–D) ((A–D): HE; magnification: ×400).

we think that the H46R and G93A transgenic rats are neuropathologically most optimal as animal models of familial ALS with the *SOD1* mutations. An essential histopathological finding of the spinal cords in ALS patients is loss of the anterior horn cells.[17] When we focus on the anterior horn cells of the spinal cords in both H46R and G93A transgenic rats, the anterior horn cells of the H46R and G93A transgenic rats are decreased before the development of clinical motor deficits. At the level of cellular pathology, the H46R and G93A transgenic rats develop Lewy body-like hyaline inclusions (LBHI) in neurons and astrocytes, which are morphological hallmarks of certain human familial ALS patients with the *SOD1* gene mutations.[17–20]

With respect to the histopathological aspects of H46R transgenic rats, the number of the anterior horn cells of the 160-day-old H46R rats that exhibit hind limb paresis is decreased with astrocytic gliosis in the spinal cords in comparison with the littermates at the same age (Fig. 3A,B). At 170 days of age when the H46R rats indicate hindlimb paraplegia sometimes associated with forelimb weakness, the histopathological finding of this clinical stage reveals more severe loss of the anterior horn cells and gliosis of the spinal cords in comparison with that of 160 days of age (Fig. 3B,C). At 200 days of age corresponding to the end-stage when the H46R rats clinically display quadriplegia or a moribund state, the H46R rats of this end-stage show severe loss of the anterior horn cells with gliosis of the spi-

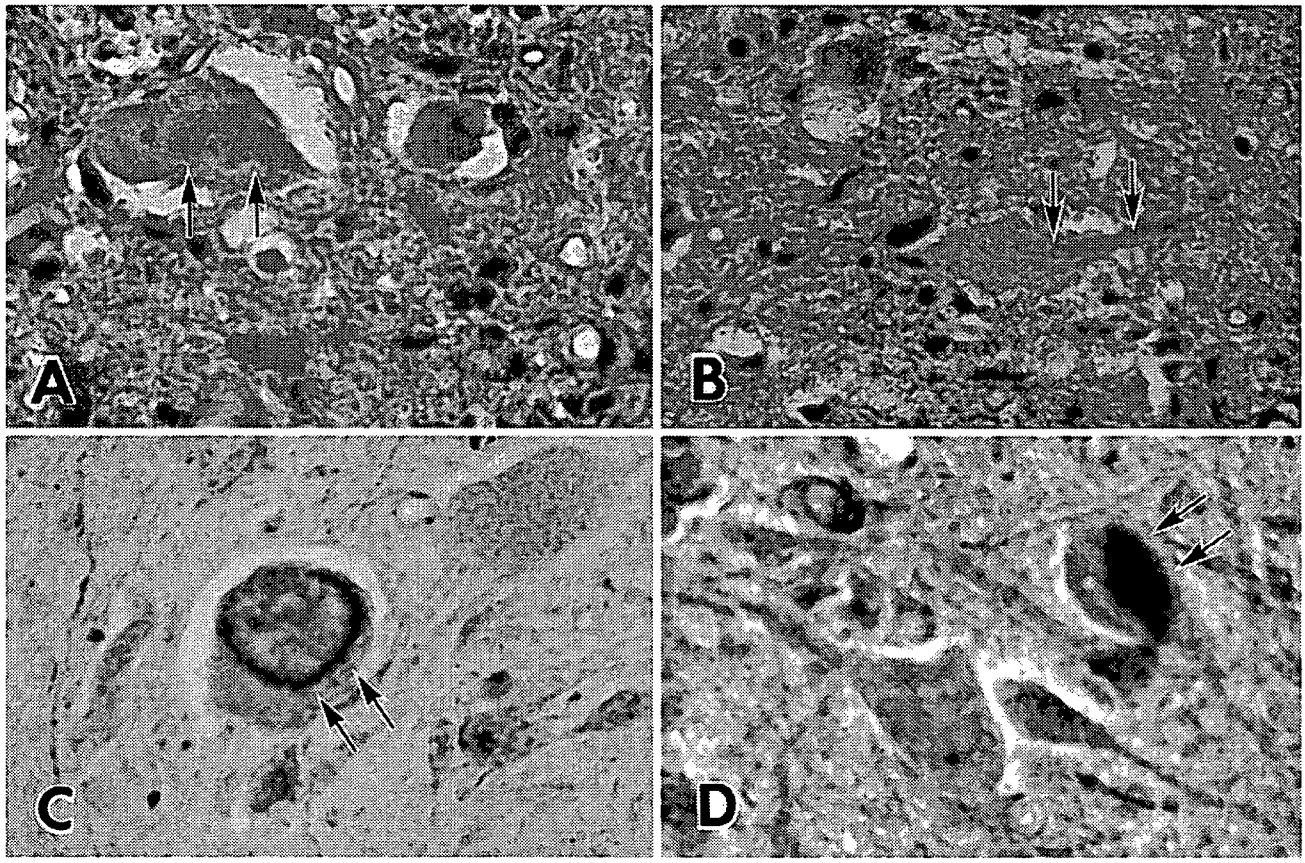

Fig. 4 Neuronal Lewy body-like hyaline inclusions (LBHI) in H46R transgenic rats. (A) A typical intracytoplasmic neuronal LBHI with a core and halo is indicated by double arrows (HE; magnification: ×820). (B) A neuronal LBHI with a core and halo is located from the cytoplasm to the dendrite (double arrows) (HE; magnification: ×820). (C) An intracytoplasmic LBHI is positive for SOD1; only the periphery of the neuronal LBHI is strongly immunostained (double arrows) (Immunostaining for SOD1; magnification: ×820). (D) An intracytoplasmic LBHI is diffusely immunostained (double arrows) (Immunostaining for SOD1; magnification: ×820). (Figure 4C is from Kato *et al.*[18] and reproduced with permission from *Acta Neuropathol*).

nal cords histopathologically compatible with those in ALS patients with clinical courses of over 5 years (Fig. 3D). As in human ALS patients, small-sized remaining anterior horn cells that appear to be normal in HE preparations are also observed throughout the disease courses in H46R and G93A transgenic rats (Fig. 3A–D).

As for the cell-pathological and immunohistochemical aspects, the rodent familial ALS model of these rats has the other important cellular pathological finding compatible with that in human familial ALS patients with the *SOD1* gene mutations; typical intracytoplasmic neuronal LBHI are observed in the remaining anterior horn cells of the spinal cords in the rat model of familial ALS. Cell-pathologically, the intracytoplasmic neuronal LBHI in the rat model of ALS are identical to those in human familial ALS. In both the rat model and human familial ALS, neuronal LBHI are formed not only in the cytoplasm but also in dendrites (Fig. 4A,B). Immunohistochemically, as in human mutant *SOD1*-mediated familial ALS,[17,19,20] the neuronal LBHI in the rat model of ALS with the H46R and G93A are positive for SOD1 (Fig. 4C,D). The reaction product deposits of the antibody against SOD1 are generally restricted to the periphery of the LBHI that show eosinophilic cores with palor peripheral halos in HE preparations (Fig. 4C). The immunostaining in intracytoplasmic and intradendtritic ill-defind LBHI is distributed throughout each of the inclusions (Fig. 4D). The rat model of ALS with the H46R and G93A also develops astrocytic hyaline inclusions (Ast-HI) that are identical structures observed in human long-term surviving familial ALS patients with the *SOD1* gene mutation.[17,19,20] In HE preparations, similarly in neuronal LBHI, Ast-HI are eosinophilic (Fig. 5A) or slightly pale inclusions and sometimes show an eosinophilic core with palor peripheral halos (Fig. 3B–D). The Ast-HI are generally round to oval and sometimes sausage-like in shape. As in neuronal LBHI, immunohistochemically, Ast-HI are intensely immunostained by the antibody against SOD1 (Fig. 5B).

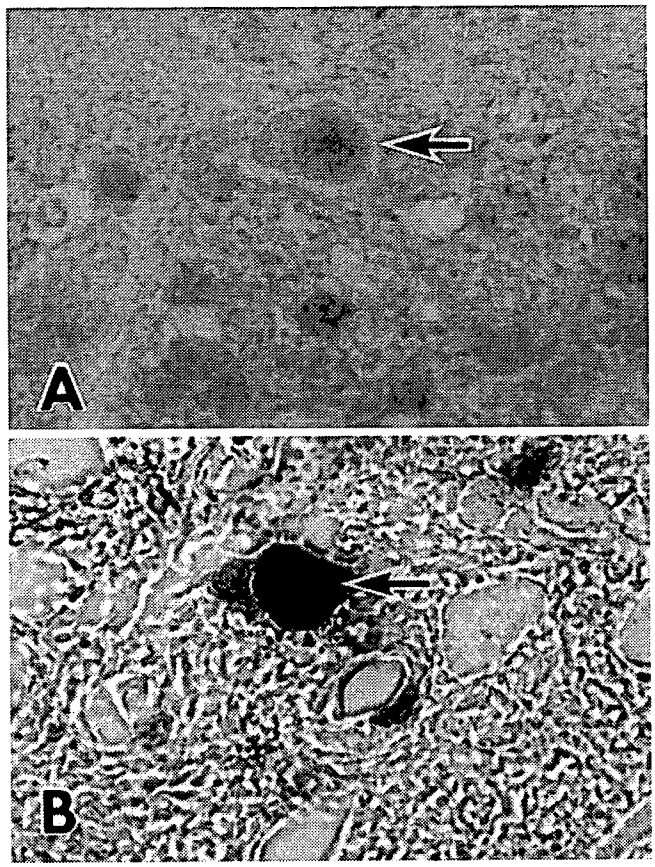

Fig. 5 Astrocytic hyaline inclusions (Ast-HI) in H46R transgenic rats. (A) Typical eosinophilic Ast-HI can be seen (arrow) (HE;magnification: ×1200). (B) An Ast-HI is strongly positive for SOD1 (arrow) (Immunostaining for SOD1;magnification: ×1200).

DISCUSSION

We have established lines of rats that express transgenes for mutant SOD1 protein with two different ALS-associated mutations: H46R and G93A. Rats with the highest transgene copy numbers and levels of expression of the mutant protein develop a paralytic disorder characterized by fulminant motor neuron death accompanied by astrogliosis and microgliosis. Particularly striking in our data is not only the earlier onset of the G93A disease but also the much more rapid course in the G93A-39 (8 days) as compared to the H46R-4 (37 days) rats. We do not understand the basis for this difference in rate of disease progression, but we note those factors determining the time course in these rats are likely to be relevant to human mutant *SOD1*-mediated familial ALS. The human H46R cases also progress very slowly, with a mean survival of 16.8 ± 6.8 years.[2,7] By contrast, the mean survival of the G93A cases in one report was 2.2 ± 1.5 years.[16] Although it is tempting to speculate that this shorter disease duration is a consequence of the higher retained dismutation activity in the G93A-39 line, we cannot firmly conclude this.

A transgenic rat model of human ALS will offer several advantages with respect to the existing transgenic mouse ALS models.[15,21] Given its larger size, it will facilitate all studies that entail CSF analysis and, in particular, those that entail multiple, serial manipulations of CSF in the same animal. Thus, it will be possible in this model to obtain adequate CSF for conventional biochemical studies as well as analyzes of small molecules and even DNA/RNA species that may distinguish the ALS from the wild-type CSF. Moreover, this model should be ideal for administration of therapies via chronic intrathecal pumps, a strategy that has been employed recently in human ALS clinical trials.[22] Another advantage of the ALS rats is that they can tolerate some forms of immunosuppressive therapy that are problematic in mice, such as cyclosporine A. This point arises in the context of an emerging interest in possible strategies to use implanted neural stem cells as therapy in ALS. It should now be possible to achieve appropriate immunosuppression in the ALS rats to allow survival of implanted cells and hence determine the efficacy of this approach. As a corollary, we also note that the larger size of the rat spinal cord will facilitate delivery of cells to the target spinal cord regions.

CONCLUSIONS

We have established lines of rats that express transgenes for mutant SOD1 protein with two different ALS-associated mutations: H46R and G93A. As in the human disease and transgenic ALS mice, pathological analysis demonstrates selective loss of motor neurons in the spinal cords of these transgenic rats. In addition, typical neuronal LBHI as well as Ast-HI identical to those in human familial ALS are observed in the spinal cords of the rats. Therefore, at present, we think that the H46R and G93A transgenic rats are neuropathologically most optimal as animal models of familial ALS with the *SOD1*-mutations.

ACKNOWLEDGMENTS

This work was supported by Grant-in-Aid from the Ministry of Health, Labour and Welfare (MA, SK, YI) and Haruki ALS Research Foundation (MA, YI).

REFERENCES

1. Brown RH Jr. Superoxide dismutase in familial amyotrophic lateral sclerosis models for gain of function. *Curr Opin Neurobiol* 1995; **5**: 841–846.
2. Aoki M, Ogasawara M, Matsubara Y *et al.* Mild ALS in Japan associated with novel SOD mutation. *Nat Genet* 1993; **5**: 323–324.

3. Rosen DR, Siddique T, Patterson D *et al.* Mutations in Cu/Zn superoxide dismutase gene are associated with familial amyotrophic lateral sclerosis. *Nature* 1993; **362**: 59–62.
4. Andersen PM, Sims KB, Xin WW *et al.* Sixteen novel mutations in the Cu/Zn superoxide dismutase gene in amyotrophic lateral sclerosis: a decade of discoveries, defects and disputes. *Amyotroph Lateral Scler Other Motor Neuron Disord* 2003; **4**: 62–73.
5. Aoki M, Abe K, Houi K *et al.* Variance of age at onset in a Japanese family with amyotrophic lateral sclerosis associated with a novel Cu/Zn superoxide dismutase mutation. *Ann Neurol* 1995; **37**: 676–679.
6. Deng HX, Tainer JA, Mitsumoto H *et al.* Two novel SOD1 mutations in patients with familial amyotrophic lateral sclerosis. *Hum Mol Genet* 1995; **4**: 1113–1116.
7. Aoki M, Ogasawara M, Matsubara Y *et al.* Familial amyotrophic lateral sclerosis (ALS) in Japan associated with H46R mutation in Cu/Zn superoxide dismutase gene: a possible new subtype of familial ALS. *J Neurol Sci* 1994; **126**: 77–83.
8. Aoki M, Abe K, Itoyama Y. Molecular analyses of the Cu/Zn superoxide dismutase gene in patients with familial amyotrophic lateral sclerosis (ALS) in Japan. *Cell Mol Neurobiol* 1998; **18**: 639–647.
9. Gurney ME, Pu H, Chiu AY *et al.* Motor neuron degeneration in mice that express a human Cu,Zn superoxide dismutase mutation. *Science* 1994; **264**: 1772–1775.
10. Wong PC, Pardo CA, Borchelt DR *et al.* An adverse property of a familial ALS-linked SOD1 mutation causes motor neuron disease characterized by vacuolar degeneration of mitochondria. *Neuron* 1995; **14**: 1105–1116.
11. Bruijn LI, Becher MW, Lee MK *et al.* ALS-linked SOD1 mutant G85R mediates damage to astrocytes and promotes rapidly progressive disease with SOD1-containing inclusions. *Neuron* 1997; **18**: 327–338.
12. Wang J, Xu G, Gonzales V *et al.* Fibrillar inclusions and motor neuron degeneration in transgenic mice expressing superoxide dismutase 1 with a disrupted copper-binding site. *Neurobiol Dis* 2002; **10**: 128–138.
13. Li M, Ona VO, Guegan C *et al.* Functional role of caspase-1 and caspase-3 in an ALS transgenic mouse model. *Science* 2000; **288**: 335–339.
14. Gurney ME, Tomasselli AG, Heinrikson RL. Stay the executioner's hand. *Science* 2000; **288**: 283–284.
15. Nagai M, Aoki M, Miyoshi I *et al.* Rats expressing human cytosolic copper-zinc superoxide dismutase transgenes with amyotrophic lateral sclerosis: associated mutations develop motor neuron disease. *J Neurosci* 2001; **21**: 9246–9254.
16. Cudkowicz M, McKenna-Yasek D, Sapp P *et al.* Epidemiology of SOD1mutations in amyotrophic lateral sclerosis. *Ann Neurol* 1997; **41**: 210–212.
17. Kato S, Shaw P, Wood-Allum C, Leigh PN, Show C. Amyotrophic lateral sclerosis. In: Dickson D (ed.) *Nerodegeneration: the Molecular Pathology of Dementia and Movement Disorders*. Basel: ISN Neuropath Press, 2003; 350–368.
18. Kato S, Saeki Y, Aoki M *et al.* Histological evidence of redox system breakdown caused by superoxide dismutase 1 (SOD1) aggregation is common to SOD1-mutated motor neurons in humans and animal models. *Acta Neuropathol* 2004; **107**: 149–158.
19. Kato S, Saito M, Hirano A, Ohama E. Recent advances in research on neuropathological aspects of familial amyotrophic lateral sclerosis with superoxide dismutase 1 gene mutations: neuronal Lewy body-like hyaline inclusions and astrocytic hyaline inclusions. *Histol Histopathol* 1999; **14**: 973–989.
20. Kato S, Takikawa M, Nakashima K *et al.* New consensus research on neuropathological aspects of familial amyotrophic lateral sclerosis with superoxide dismutase 1 (SOD1) gene mutations: inclusions containing SOD1 in neurons and astrocytes. *Amyotroph Lateral Scler Other Motor Neuron Disord* 2000; **1**: 163–184.
21. Howland DS, Liu J, She Y *et al.* Focal loss of the glutamate transporter EAAT2 in a transgenic rat model of SOD1 mutant-mediated amyotrophic lateral sclerosis (ALS). *Proc Natl Acad Sci USA* 2002; **99**: 1604–1609.
22. Mitsumoto H, Gordon P, Kaufmann P, Gooch CL, Przedborski S, Rowland LP. Randomized control trials in ALS: lessons learned. *Amyotroph Lateral Scler Other Motor Neuron Disord* 2004; **5** (Suppl. 1): 8–13.

Journal of Neuroscience Research 82:63–70 (2005)

Motoneuron Degeneration After Facial Nerve Avulsion Is Exacerbated in Presymptomatic Transgenic Rats Expressing Human Mutant Cu/Zn Superoxide Dismutase

Ken Ikeda,[1,2] Masashi Aoki,[3] Yoko Kawazoe,[1] Tsuyoshi Sakamoto,[1] Yuichi Hayashi,[1] Aya Ishigaki,[3] Makiko Nagai,[3] Rieko Kamii,[3] Shinsuke Kato,[4] Yasuto Itoyama,[3] and Kazuhiko Watabe[1]*

[1]Department of Molecular Neuropathology, Tokyo Metropolitan Institute for Neuroscience, Tokyo, Japan
[2]Department of Neurology, PL Tokyo Health Care Center, Tokyo, Japan
[3]Department of Neurology, Tohoku University Graduate School of Medicine, Sendai, Japan
[4]Department of Neuropathology, Institute of Neurological Sciences, Faculty of Medicine, Tottori University, Yonago, Japan

We investigated motoneuron degeneration after proximal nerve injury in presymptomatic transgenic (tg) rats expressing human mutant Cu/Zn superoxide dismutase (SOD1). The right facial nerves of presymptomatic tg rats expressing human H46R or G93A SOD1 and their non-tg littermates were avulsed, and facial nuclei were examined at 2 weeks postoperation. Nissl-stained cell counts revealed that facial motoneuron loss after avulsion was exacerbated in H46R- and G93A-tg rats compared with their non-tg littermates. The loss of motoneurons in G93A-tg rats after avulsion was significantly greater than that in H46R-tg rats. Intense cytoplasmic immunolabeling for SOD1 in injured motoneurons after avulsion was demonstrated in H46R- and G93A-tg rats but not in their littermates. Facial axotomy did not induce significant motoneuron loss nor enhance SOD1 immunoreactivity in these tg rats and non-tg littermates at 2 weeks postoperation, although both axotomy and avulsion elicited intense immunolabeling for activating transcription factor-3, phosphorylated c-Jun, and phosphorylated heat shock protein 27 in injured motoneurons of all these animals. The present data indicate the increased vulnerability of injured motoneurons after avulsion in the presymptomatic mutant SOD1-tg rats.

Key words: axotomy; facial nerve; amyotrophic lateral sclerosis; ALS; mutant Cu/Zn superoxide dismutase; SOD1; transgenic rat

Since the discovery of the mutation of Cu/Zn superoxide dismutase (SOD1) in patients with familial amyotrophic lateral sclerosis (ALS) and the development of transgenic (tg) mice and rats expressing human mutant SOD1 that show clinicopathological characteristics comparable to human familial ALS, the mutant SOD1-tg animals have been the most widely used experimental models for elucidating the pathomechanism of and the therapeutic approach for familial ALS as well as sporadic ALS (Cleveland and Rothstein, 2001). Although the precise mechanism of motoneuron degeneration in mutant SOD1-tg animals is largely unknown, the mutant SOD1 is thought to have a gain of toxic function (Cleveland and Rothstein, 2001). In another animal model of motoneuron degeneration, peripheral nerve avulsion exhibits extensive loss of motoneurons in adult rats (Søreide, 1981; Wu, 1993; Koliatsos et al., 1994; Watabe et al., 2000; Sakamoto et al., 2000, 2003a,b; Ikeda et al., 2003; Moran and Graeber, 2004). The mechanism of motoneuron degeneration after avulsion also remains unclear, but peroxinitrite-mediated oxidative damage and perikaryal accumulation of phosphorylated neurofilaments have been demonstrated in injured motoneurons after avulsion (Martin et al., 1999). Both of these pathological features have also been shown in

Contract grant sponsor: Ministry of Education, Culture, Sports, Science and Technology, Japan; Contract grant sponsor: Research on Specific Diseases, Health Sciences Research Grants, Ministry of Health, Labor and Welfare, Japan; Contract grant sponsor: Research on Psychiatric and Neurological Diseases and Mental Health, H16-kokoro-017, Ministry of Health, Labor and Welfare, Japan.

*Correspondence to: Kazuhiko Watabe, MD, PhD, Department of Molecular Neuropathology, Tokyo Metropolitan Institute for Neuroscience, 2-6 Musashidai, Fuchu, Tokyo 183-8526, Japan.
E-mail: kazwtb@tmin.ac.jp

Received 6 April 2005; Revised 31 May 2005; Accepted 30 June 2005

Published online 17 August 2005 in Wiley InterScience (www.interscience.wiley.com). DOI: 10.1002/jnr.20621

spinal motoneurons in mutant SOD1-tg animals as well as in patients with familial and sporadic ALS (Estévez et al., 1998; Cleveland, 1999; Cleveland and Rothstein, 2001). If motoneuron degeneration after peripheral nerve avulsion shares any underlying mechanisms of motoneuron death associated with SOD1 mutation, motoneurons in presymptomatic mutant SOD1-tg animals may be more susceptible to pathological insults following avulsion compared with their non-tg littermates. If this is so, we may be able to utilize facial nerve avulsion as an animal model for understanding the mechanisms of motoneuron degeneration in ALS. In the present study, we examined injured motoneurons after facial nerve avulsion in presymptomatic mutant human SOD1-tg rats and their littermates.

MATERIALS AND METHODS

Animals and Surgical Procedures

The experimental protocols were approved by the Institutional Animal Care and Use Committee of Tokyo Metropolitan Institute for Neuroscience and Tohoku University Graduate School of Medicine. The tg rats expressing human mutant SOD1 (H46R, G93A) were generated as described previously (Nagai et al., 2001). Two types of rats with SOD1 mutations, H46R and G93A, were used for experiments. The H46R-tg rats develop motor deficits at about 140 days of age and die after 3 weeks, and G93A-tg rats show the clinical signs at around 120 days of age and die after 10 days (Nagai et al., 2001).

The presymptomatic female H46R (90 days old)- and G93A (80 days old)-tg rats were anesthetized with inhalation of halothane. Under a dissecting microscope, the right facial nerve was exposed at its exit from the stylomastoid foramen. With microhemostat forceps, the proximal facial nerve was avulsed by gentle traction and removed from the distal facial nerve as described elsewhere (Sakamoto et al., 2000, 2003a,b; Ikeda et al., 2003). As for axotomy, the right facial nerve was transected at its exit from the stylomastoid foramen, and a distal portion of the nerve, 5 mm in length, was cut and removed. The wound was covered with a small piece of gelatin sponge (Gelfoam; Pharmacia Upjohn, Bridgewater, NJ) and closed by fine suture.

Motoneuron Cell Counting

At 2 weeks postoperation, rats were anesthetized with a lethal dose of pentobarbital sodium and transcardially perfused with 0.1 M phosphate buffer, pH 7.4 (PB), followed by 4% paraformaldehyde in 0.1 M PB. The brainstem tissue was excised, postfixed in the same fixative for 2 hr, dehydrated, and embedded in paraffin, and serial transverse sections (6-μm thickness) were made. Every fifth section (24-μm interval) was collected, deparaffinized, and stained with cresyl violet (Nissl staining), and facial motoneurons having nuclei containing distinct nucleoli on both sides of the facial nuclei were counted in 25 sections as described elsewhere (Sakamoto et al., 2000, 2003a,b; Ikeda et al., 2003). The data were expressed as the mean ± SEM, and statistical significance was assessed by Mann-Whitney U-test.

Immunohistochemistry

Immunohistochemistry on paraffin sections was performed with the following primary antibodies: sheep anti-human SOD1 (1:1,000; Calbiochem, San Diego, CA), rabbit anti-human SOD1 (1:10,000; kindly provided by Dr. K. Asayama; Asayama and Burr, 1984), mouse monoclonal anti-phosphorylated neurofilament SMI-31 (1:1,000; Sternberger Monoclonals, Lutherville, MD), rabbit anti-ubiquitin (1:1,000; Dako, Glostrup, Denmark), rabbit anti-glial fibrillary acidic protein (GFAP; 1:1,000; Dako), rabbit anti-activating transcription factor-3 (ATF3; sc-188, 1:200; Santa Cruz Biotechnology, Santa Cruz, CA), rabbit anti-c-Jun (sc-1694, 1:200; Santa Cruz Biotechnology), mouse monoclonal anti-phosphorylated c-Jun (sc-822, 1:200; Santa Cruz Biotechnology), rabbit anti-heat shock protein (Hsp) 25 that reacts with rat Hsp27 (SPA-801, 1:200; Stressgen, Victoria, British Columbia, Canada), and rabbit anti-phosphospecific (Ser^{15})Hsp27 (1:200; Oncogene, San Diego, CA). For immunohistochemistry, deparaffinized sections were pretreated with 0.3% H_2O_2 in methanol and preincubated with 3% heat-inactivated goat or rabbit serum in 0.1% Triton X-100 in phosphate-buffered saline (T-PBS). In cases of immunostaining with mouse primary antibodies, MOM blocking kit (Vector, Burlingame, CA) was used according to the manufacturer's instructions to reduce nonspecific background staining. Sections were then incubated overnight at 4°C with the primary antibodies diluted in T-PBS, followed by the incubation with biotinylated rabbit anti-sheep, goat anti-rabbit, or goat anti-mouse IgG at a dilution of 1:200 and with ABC reagent (Vector), visualized by 3,3′-diaminobenzidine tetrahydrocholoride (DAB)-H_2O_2 solution and counterstained with hematoxylin. For negative controls, the primary antibodies were omitted or replaced by nonimmunized animal sera.

RESULTS

Two weeks after avulsion of the right facial nerves in non-tg littermates, the number of surviving facial motoneurons declined to ~70% of that on the contralateral side, similar to that in normal rats, as described previously (Sakamoto et al., 2000). In SOD1-tg rats, only ~30–50% of motoneurons survived 2 weeks after avulsion, indicating that the loss of motoneurons was exacerbated in SOD1-tg rats compared with their non-tg littermates (Fig. 1, Table I). The numbers of surviving motoneurons in G93A-tg rats after avulsion (~35% of contralateral side) were significantly less than those in H46R-tg rats (~50% of contralateral side; Table I). The numbers of intact motoneurons at contralateral sides did not differ between tg rats and non-tg littermates, indicating that cell loss does not happen at this moment in the course of the disease with SOD1 mutations (Table I). Facial nerve axotomy did not induce significant loss of injured motoneurons in tg rats and non-tg littermates at 2 weeks postoperation (Fig. 1, Table I).

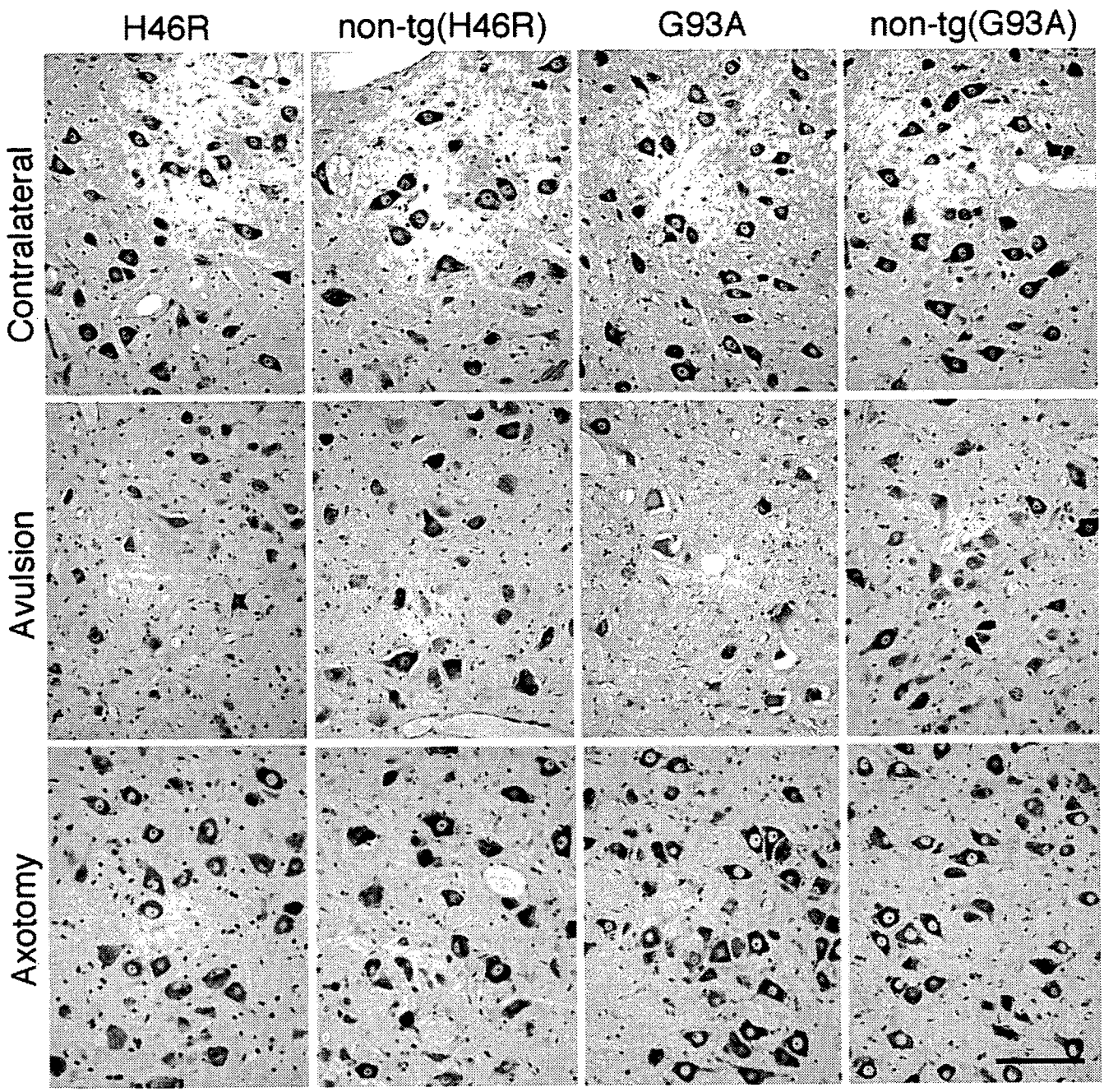

Fig. 1. Facial motoneurons of H46R- and G93A-transgenic (tg) rats and their non-tg littermates on the contralateral and ipsilateral (avulsion or axotomy) sides 2 weeks after facial nerve avulsion or axotomy. Nissl stain. Scale bar = 100 μm.

Examination of sections immunostained for SOD1 showed intense cytoplasmic immunolabeling for SOD1 in injured motoneurons after avulsion in H46R- and G93A-tg rats compared with uninjured motoneurons on the contralateral side that were not or were very faintly immunoreactive for SOD1 (Fig. 2). We used sheep and rabbit anti-SOD1 antibodies, both of which gave identical results. The cytoplasmic SOD1 immunolabeling patterns of injured motoneurons appeared diffuse in H46R-tg rats, whereas they were granular in G93A-tg rats. In G93A-tg rats, there were axons and vacuolar changes in the neuropil consistently immunoreactive for SOD1 at both uninjured and injured sides of facial nuclei (Fig. 2). There was no definite immunolabeling for SOD1 in either injured or uninjured motoneurons and their axons in non-tg littermates (Fig. 2). Facial nerve axotomy did not increase immunoreactivity for SOD1 in injured motoneurons of tg rats and non-tg littermates at 2 weeks

TABLE I. Survival of Motoneurons After Facial Nerve Avulsion and Axotomy†

Rat (n)	Ipsilateral motoneuron number	Contralateral motoneuron number	Survival %
Avulsion			
NL (H46R) (n = 10)	598 ± 18	813 ± 26	73.7 ± 1.2
H46R (n = 8)	402 ± 36*	839 ± 27	47.5 ± 2.8*
NL (G93A) (n = 6)	637 ± 56	822 ± 47	76.7 ± 3.0
G93A (n = 7)	306 ± 37*	884 ± 44	34.7 ± 3.6*,**
Axotomy			
H46R (n = 5)	751 ± 19	843 ± 23	89.2 ± 1.4
NL (G93A) (n = 6)	743 ± 15	835 ± 12	88.9 ± 0.6
G93A (n = 5)	741 ± 42	781 ± 45	94.9 ± 1.2

†Numbers of facial motoneurons and the percent survival at the ipsilateral (lesion) side relative to the contralateral (control) side 2 weeks after avulsion or axotomy. Results are presented as mean ± SEM. Statistical comparison was done by Mann-Whitney U-test. n = number of animals. NL. nontransgenic littermates.
*$P < 0.01$ vs. NL (H46R) and NL (G93A) rats after avulsion.
**$P < 0.05$ vs. H46R-transgenic rats after avulsion.

postoperation (Fig. 2). In contrast, immunohistochemical examination showed perikaryal accumulation of phosphorylated neurofilaments in injured motoneurons both after axotomy and after avulsion, as described previously (Koliatsos et al., 1989, 1994; Koliatsos and Price, 1996). There were no hyaline inclusions identifiable in HE-stained sections or ubiquitin-immunoreactive structures in both H46R- and G93A-tg rats and their non-tg littermates on either operated or contralateral sides (data not shown). Proliferation of astrocytes as evidenced by immunostaining for GFAP was observed at the injured sides in all the animals after avulsion and axotomy, and the degree of the astrocytic response appeared to correlate with the extent of motoneuron loss after avulsion; i.e., more intense GFAP immunostaining was demonstrated when less neuronal survival was observed (Fig. 3).

It has been shown that ATF3 is expressed, and c-Jun and Hsp27 are up-regulated and phosphorylated, in injured motoneurons after axotomy (Tsujino et al., 2000; Casanovas et al., 2001; Benn et al., 2002; Kalmár et al., 2002). Several reports have documented that ATF3, c-Jun, and Hsp27 cooperate to promote neuronal survival in vitro and in vivo, suggesting neuroprotective roles of these molecules (Pearson et al., 2003; Nakagomi et al., 2003). We then examined the expression of ATF3, c-Jun, and Hsp27 in injured motoneurons after facial nerve avulsion that causes extensive neuronal loss. In wild-type adult rats, intact facial motoneurons were constitutively immunoreactive for c-Jun and Hsp27 but not for ATF3, phosphorylated c-Jun, or phosphorylated Hsp27, whereas injured motoneurons become immunoreactive for ATF3, phosphorylated c-Jun, and phosphorylated Hsp27 within 1 day after facial nerve avulsion and remain positive up to 4 weeks (Watabe et al., unpublished observations). In a similar manner, virtually all injured motoneurons were immunostained for ATF3, phosphorylated c-Jun, and phosphorylated Hsp27 in H46R- and G93A-tg rats and their non-tg littermates 2 weeks after avulsion and axotomy as examined in this study (Fig. 3).

DISCUSSION

We demonstrated that only 50% (H46R-tg rats) or 35% (G93A-tg rats) of motoneurons in mutant SOD1-tg rats survived 2 weeks after avulsion at their presymptomatic stage compared with 70% survival of motoneurons in their non-tg littermates, indicating that motoneuron degeneration after avulsion is significantly more severe in these presymptomatic mutant SOD1-tg rats. It is interesting to note that the loss of motoneurons in G93A-tg rats was significantly greater than that in H46R-tg rats after avulsion, insofar as the onset of paralysis is earlier and the disease progression is more rapid in G93A-tg rats compared with the H46R rats used in the present study (Nagai et al., 2001). The clinical courses of these tg rats are also likely to be relevant to those of human mutant SOD1-mediated familial ALS, in that the human H46R cases progress very slowly compared with the G93A cases (Nagai et al., 2001; Aoki et al., 1993, 1994). In contrast, we did not see significant motoneuron loss in the presymptomatic SOD1-tg rats and their non-tg littermates 2 weeks after facial nerve axotomy. Unlike avulsion, axotomy does not generally induce significant motoneuron death in adult rodents (Lowrie and Vrbová, 1992; Moran and Graeber, 2004), except that, in the case of adult Balb/C mice, the facial nerve axotomy leads to loss of >50% of the motoneurons at 30 days postoperation (Hottinger et al., 2000), and C57BL mice show late motoneuron loss (~60%) 8 weeks after facial nerve axotomy (Angelov et al., 2003). Mariotti et al. (2002) axotomized facial nerves of G93A-tg mice and their non-tg littermates at their presymptomatic stage and observed loss of facial motoneurons that was higher in G93A-tg mice than in non-tg littermates at 30 days postaxotomy; these data are relevant to our present data acquired from avulsion, but not axotomy, in rats, which probably is due to the use of different animal species. In contrast, Kong and Xu (1999) described axotomy of lumbar spinal or sciatic nerve in G93A-tg mice at the presymptomatic stage reducing the extent of axon degeneration at the end stage of the disease. They did

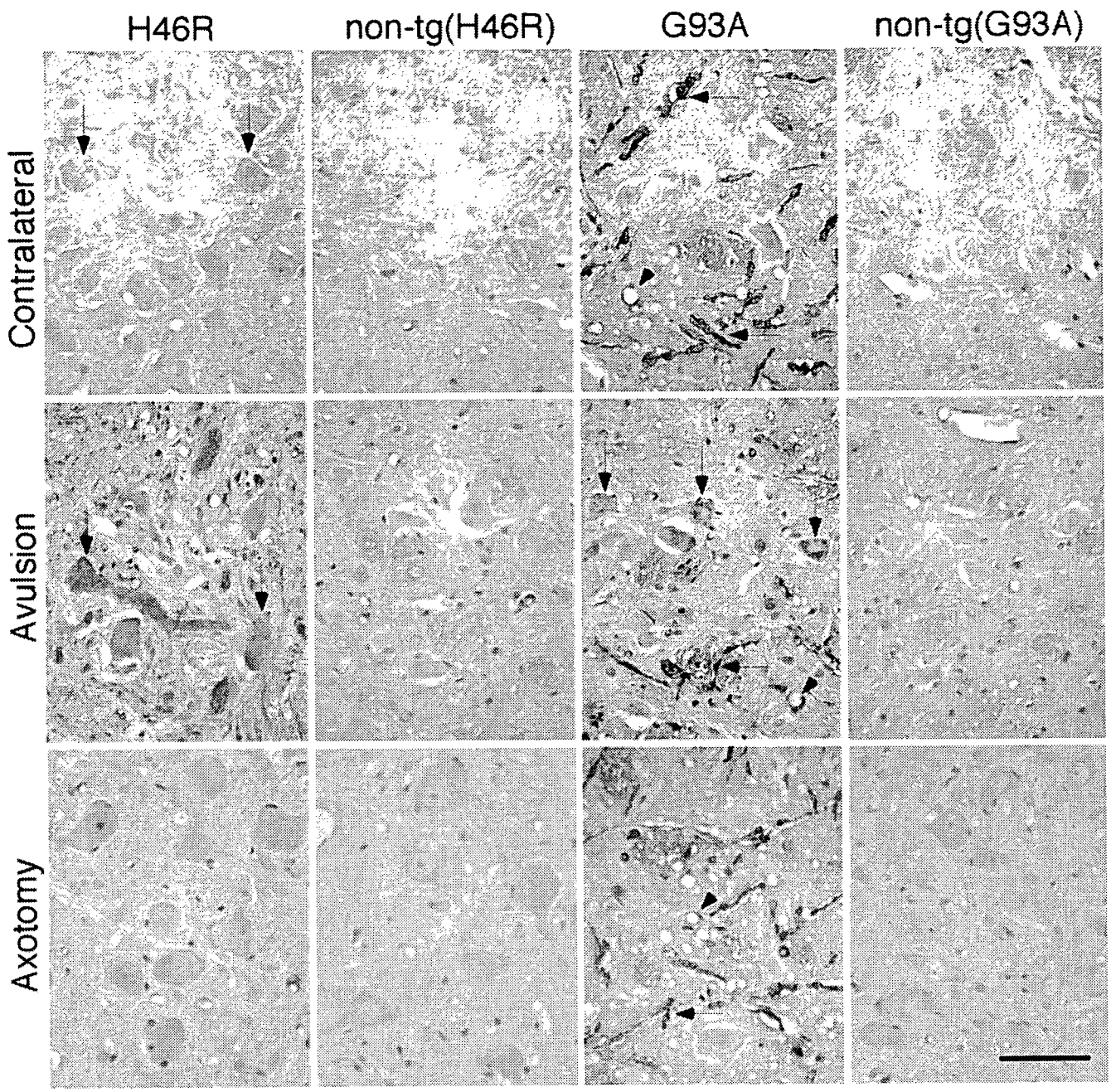

Fig. 2. SOD1 immunohistochemistry of facial motoneurons of H46R- and G93A-tg rats and their non-tg littermates on the contralateral and ipsilateral (avulsion or axotomy) sides 2 weeks after facial nerve avulsion or axotomy. Counterstained with hematoxylin. Note immunostained motoneurons (vertical arrows), axons (horizontal arrows), and vacuoles in neuropil (arrowheads) in H46R- and G93A-tg rats. Scale bar = 50 μm.

not evaluate the response of the cell bodies of spinal motoneurons, so it remains unknown whether SOD1 mutation affects the viability of spinal motoneurons after axotomy. In the present study, we demonstrated that motoneuron degeneration after facial nerve avulsion, but not after axotomy, is exacerbated in presymptomatic mutant SOD1-tg rats at 2 weeks postoperation. These data clearly indicate the increased vulnerability of facial motoneurons to proximal nerve injury in the presymptomatic SOD1-tg rats.

It has been shown that SOD1 is abundantly expressed in cell bodies, dendrites, and axons of wild-type mouse and rat motoneurons in vivo (Pardo et al., 1995; Moreno et al., 1997; Yu, 2002). In the present

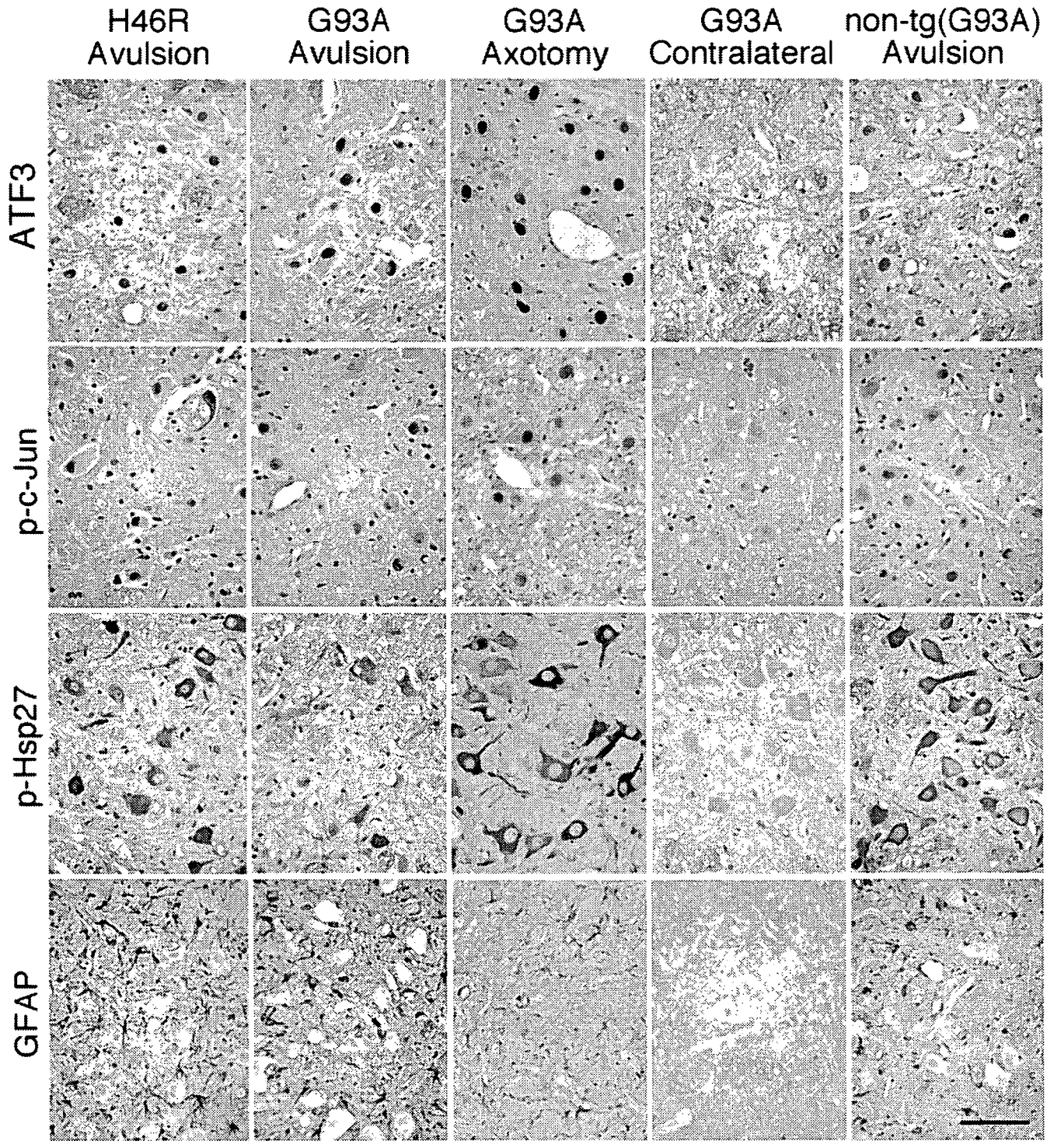

Fig. 3. Immunohistochemistry for ATF3, phosphorylated c-Jun (p-c-Jun), phosphorylated Hsp27 (p-Hsp27), and GFAP of facial nuclei in H46R-tg rat, G93A-tg rat, and non-tg littermate on the ipsilateral (avulsion or axotomy) and contralateral sides 2 weeks after facial nerve avulsion or axotomy. All injured motoneurons are immunostained for ATF3, phosphorylated c-Jun, and phosphorylated Hsp27 in these rats after avulsion or axotomy. The intensity of GFAP immunoreactivity appears parallel to the extent of motoneuron loss (see also Fig. 1). Counterstained with hematoxylin. Scale bar = 50 μm.

study, we did not observe immunoreactivity for SOD1 in facial motoneurons of nontransgenic littermates with sheep and rabbit anti-human SOD1 antibodies; it is postulated that the antibody concentrations (i.e., 1:1,000–10,000) used in this study are below the detection levels for immunostaining rat SOD1 antigen on paraffin sections. Instead, we demonstrated some facial motoneurons showing very faint immunoreactivity for SOD1 in H46R-tg rats on paraffin sections. In G93A-tg rats, axons and vacuoles in neuropil were intensely immunoreactive for SOD1 at both uninjured and injured sides. The increased immunostaining for SOD1 in injured motoneurons of SOD1 (H46R and G93A)-tg rats may therefore indicate that human mutant SOD1 protein is accumulated in the cytoplasm of facial motoneurons after avulsion. When several mutant SOD1 genes that include G93A were transfected to COS7 cells, the mutant SOD1s, but not wild-type SOD1, aggregated in association with the endoplasmic reticulum (ER) and induced ER stress (Tobisawa et al., 2003). Accumulation of mutant SOD1 in injured motoneurons after avulsion may therefore potentiate ER stress and exacerbate motoneuron death in the presymptomatic mutant SOD1-tg rats, although the mechanism of accumulation of SOD1 remains unknown. Whether up-regulation of cytoplasmic mutant SOD1 expression or retrograde accumulation of mutant SOD1 from injured axons was induced in these neurons awaits further investigations. In addition, facial nerve axotomy, as opposed to avulsion, did not increase immunoreactivity for SOD1 in injured motoneurons of SOD1-tg rats and their non-tg littermates, which seems consistent with the absence of significant motoneuron loss in these rats as described above. As for wild-type SOD1, previous reports documented no change in SOD1 mRNA levels or SOD1 immunoreactivity in injured motoneurons after facial or sciatic nerve axotomy in wild-type rats (Yoneda et al., 1992; Rosefeld et al., 1997).

It has been demonstrated that ATF3 is expressed, and c-Jun and Hsp27 are up-regulated and phosphorylated, in injured adult motoneurons after axotomy (Tsujino et al., 2000; Casanovas et al., 2001; Benn et al., 2002; Kalmár et al., 2002). As for the neuroprotective nature of these molecules, it has been reported that ATF3 enhances c-Jun-mediated neurite sprouting in PC12 and Neuro-2a cells (Pearson et al., 2003), and ATF3 and Hsp27 cooperate with c-Jun to prevent death of PC12 cells and superior cervical ganglion neurons (Nakagomi et al., 2003). Hsp27 is induced and phosphorylated in adult, but not in neonatal, motoneurons after axotomy, and axotomized neonatal motoneurons that lack Hsp27 die by apoptosis, suggesting that phosphorylated Hsp27 is necessary for motoneuron survival after peripheral nerve injury (Benn et al., 2002). However, there have been no reports concerning the expression of ATF3, phosphorylated c-Jun, and phosphorylated Hsp27 in injured motoneurons after avulsion. In the present study, we have demonstrated that, even after avulsion that causes extensive motoneuron death, ATF3, phosphorylated c-Jun, and phosphorylated Hsp27 were fully up-regulated in both SOD1-tg and non-tg rats. These results suggest that neuroprotective effects of Hsp27 cannot overcome yet unidentified stress(es) induced by facial nerve avulsion. On the other hand, a recent report demonstrated that facial motoneurons of c-Jun-deficient mice are resistant to axotomy-induced cell death, suggesting that c-Jun promotes posttraumatic motoneuron death (Raivich et al., 2004). In addition, it has been shown that mutant SOD1 binds to Hsp27 and forms aggregates, suggesting that this binding of Hsp27 to mutant SOD1 blocks antiapoptotic function of Hsp27 and leads to motoneuron death (Okado-Matsumoto and Fridovich, 2002). The effects of phosphorylated c-Jun and Hsp27 and their association with mutant SOD1 accumulation should be further investigated to elucidate the mechanism of exacerbated motoneuron death in SOD1-tg rats after avulsion.

In this study, we have demonstrated that motoneuron degeneration after facial nerve avulsion is exacerbated in presymptomatic mutant SOD1-tg rats compared with their non-tg littermates. Mutant SOD1 accumulation and its association with c-Jun and Hsp27 may have a key role leading to enhanced motoneuron death. In this context, motoneuron death after avulsion may share, at least in part, a common mechanism with the motoneuron degeneration associated with SOD1 mutation.

ACKNOWLEDGMENT

We are grateful to Dr. Kohtaro Asayama (University of Occupational and Environmental Health, Japan) for kindly providing rabbit anti-SOD1 antibody.

REFERENCES

Angelov DN, Waibel S, Guntinas-Lichius O, Lenzen M, Neiss WF, Tomov TL, Yoles E, Kipnis J, Schori H, Reuter A, Ludolph A, Schwartz M. 2003. Therapeutic vaccine for acute and chronic motor neuron diseases: implications for amyotrophic lateral sclerosis. Proc Natl Acad Sci U S A 100:4790–4795.

Aoki M, Ogasawara M, Matsubara Y, Narisawa K, Nakamura S, Itoyama Y, Abe K. 1993. Mild ALS in Japan associated with novel SOD mutation. Nat Genet 5:323–324.

Aoki M, Ogasawara M, Matsubara Y, Narisawa K, Nakamura S, Itoyama Y, Abe K. 1994. Familial amyotrophic lateral sclerosis (ALS) in Japan associated with H46R mutation in Cu/Zn superoxide dismutase gene: a possible new subtype of familial ALS. J Neurol Sci 126:77–83.

Asayama K, Burr IM. 1984. Joint purification of mangano and copper/zinc superoxide dismutase from a single source: a simplified method. Anal Biochem 136:336–339.

Benn SC, Perrelet D, Kato AC, Scholz J, Decosterd I, Mannion RJ, Bakowska JC, Woolf CJ. 2002. Hsp27 upregulation and phosphorylation is required for injured sensory and motor neuron survival. Neuron 36:45–56.

Casanovas A, Ribera J, Hager G, Kreutzberg GW, Esquerda JE. 2001. c-Jun regulation in rat neonatal motoneurons postaxotomy. J Neurosci 63:469–479.

Cleveland DW. 1999. From Charcot to SOD1: mechanisms of selective motor neuron death in ALS. Neuron 24:515–520.

Cleveland DW, Rothstein JD. 2001. From Charcot to Lou Gehrig: deciphering selective motor neuron death in ALS. Nat Rev Neurosci 2:806–819.

Estévez AG, Spear N, Manuel SM, Barbeito L, Radi R, Beckman JS. 1998. Role of endogenous nitric oxide and peroxynitrite formation in the survival and death of motor neurons in culture. Prog Brain Res 18: 269–280.

Hottinger AF, Azzouz M, Déglon N, Aebischer P, Zurn AD. 2000. Complete and long-term rescue of lesioned adult motoneurons by lentiviral-mediated expression of glial cell line-derived neurotrophic factor in the facial nucleus. J Neurosci 20:5587–5593.

Ikeda K, Sakamoto T, Kawazoe Y, Marubuchi S, Nakagawa M, Ono S, Terashima N, Kinoshita M, Iwasaki Y, Watabe K. 2003. Oral administration of a neuroprotective compound T-588 prevents motoneuron degeneration after facial nerve avulsion in adult rats. Amyotroph Lateral Scler Other Motor Neuron Disord 4:74–80.

Kalmár B, Burnstock G, Vrbová G, Greensmith L. 2002. The effect of neonatal injury on the expression of heat shock proteins in developing rat motoneurons. J Neurotrauma 19:667–679.

Koliatsos VE, Price DL. 1996. Axotomy as an experimental model of neuronal injury and cell death. Brain Pathol 6:447–465.

Koliatsos VE, Applegate MD, Kitt CA, Walker LC, DeLong MR, Price DL. 1989. Aberrant phosphorylation of neurofilaments accompanies transmitter-related changes in rat septal neurons following transection of the fimbria-fornix. Brain Res 482:205–218.

Koliatsos VE, Price WL, Pardo CA, Price DL. 1994. Ventral root avulsion: an experimental model of death of adult motor neurons. J Comp Neurol 342:35–44.

Kong J, Xu Z. 1999. Peripheral axotomy slows motoneuron degeneration in a transgenic mouse line expressing mutant SOD1 G93A. J Comp Neurol 412:373–380.

Lowrie MB, Vrbová G. 1992. Dependence of postnatal motoneurones on their targets: review and hypothesis. Trend Neurosci 15:80–84.

Mariotti R, Cristino L, Bressan C, Boscolo B, Bentivoglio M. 2002. Altered reaction of facial motoneurons to axonal damage in the presymptomatic phase of a murine model of familial amyotrophic lateral sclerosis. Neuroscience 115:331–335.

Martin LJ, Kaiser A, Price AC. 1999. Motor neuron degeneration after nerve avulsion in adult evolves with oxidative stress and is apoptosis. J Neurobiol 40:185–201.

Moran LB, Graeber MB. 2004. The facial nerve axotomy model. Brain Res Rev 44:154–178.

Moreno S, Nardacci R, Ceru MP. 1997. Regional and ultrastructural immunolocalization of copper-zinc superoxide dismutase in rat central nervous system. J Histochem Cytochem 45:1611–1633.

Nagai M, Aoki M, Miyoshi I, Kato M, Pasinelli P, Kasai N, Brown RH Jr, Itoyama Y. 2001. Rats expressing human cytosolic copper-zinc superoxide dismutase transgenes with amyotrophic lateral sclerosis: associated mutations develop motor neuron disease. J Neurosci 21:9246–9254.

Nakagomi S, Suzuki Y, Namikawa K, Kiryu-Seo S, Kiyama H. 2003. Expression of the activating transcription factor 3 prevents c-Jun N-terminal kinase-induced neuronal death by promoting heat shock protein 27 expression and Akt activation. J Neurosci 23:5187–5196.

Okado-Matsumoto A, Fridovich I. 2002. Amyotrophic lateral sclerosis: a proposed mechanism. Proc Natl Acad Sci U S A 99:9010–9014.

Pardo CA, Xu Z, Borchelt DR, Price DL, Sisodia SS, Cleveland DW. 1995. Superoxide dismutase is an abundant component in cell bodies, dendrites, and axons of motor neurons and in a subset of other neurons. Proc Natl Acad Sci U S A 92:954–958.

Pearson AG, Gray CW, Pearson JF, Greenwood JM, During MJ, Dragunow M. 2003. ATF3 enhances c-Jun-mediated neurite sprouting. Brain Res Mol Brain Res 120:38–45.

Raivich G, Bohatschek M, Da Costa C, Iwata O, Galiano M, Hristova M, Nateri AS, Makwana M, Riera-Sans L, Wolfer DP, Lipp HP, Aguzzi A, Wagner EF, Behrens A. 2004. The AP-1 transcription factor c-Jun is required for efficient axonal regeneration. Neuron 43:57–67.

Rosenfeld J, Cook S, James R. 1997. Expression of superoxide dismutase following axotomy. Exp Neurol 147:37–47.

Sakamoto T, Watabe K, Ohashi T, Kawazoe Y, Oyanagi K, Inoue K, Eto Y. 2000. Adenoviral vector-mediated GDNF gene transfer prevents death of adult facial motoneurons. Neuroreport 11:1857–1860.

Sakamoto T, Kawazoe Y, Shen J-S, Takeda Y, Arakawa Y, Ogawa J, Oyanagi K, Ohashi T, Watanabe K, Inoue K, Eto Y, Watabe K. 2003a. Adenoviral gene transfer of GDNF, BDNF and TGFβ2, but not CNTF, cardiotrophin-1 or IGF1, protects injured adult motoneurons after facial nerve avulsion. J Neurosci Res 72:54–64.

Sakamoto T, Kawazoe Y, Uchida Y, Hozumi I, Inuzuka T, Watabe K. 2003b. Growth inhibitory factor prevents degeneration of injured adult rat motoneurons. Neuroreport 14:2147–2151.

Søreide AJ. 1981. Variations in the axon reaction after different types of nerve lesion. Acta Anat 110:173–188.

Tobisawa S, Hozumi Y, Arawaka S, Koyama S, Wada M, Nagai M, Aoki M, Itoyama Y, Goto K, Kato T. 2003. Mutant SOD1 linked to familial amyotrophic lateral sclerosis, but not wild-type SOD1, induces ER stress in COS7 cells and transgenic mice. Biochem Biophys Res Commun 303:496–503.

Tsujino H, Kondo E, Fukuoka T, Dai Y, Tokunaga A, Miki K, Yonenobu K, Ochi T, Noguchi K. 2000. Activating transcription factor 3 (ATF3) induction by axotomy in sensory and motoneurons: a novel neuronal marker of nerve injury. Mol Cell Neurosci 15:170–182.

Watabe K, Ohashi T, Sakamoto T, Kawazoe Y, Takeshima T, Oyanagi K, Inoue K, Eto Y, Kim SU. 2000. Rescue of lesioned adult rat spinal motoneurons by adenoviral gene transfer of glial cell line-derived neurotrophic factor. J Neurosci Res 60:511–519.

Wu W. 1993. Expression of nitric-oxide synthase (NOS) in injured CNS neurons as shown by NADPH diaphorase histochemistry. Exp Neurol 120:153–159.

Yoneda T, Inagaki S, Hayashi Y, Nomura T, Takagi H. 1992. Differential regulation of manganese and copper/zinc superoxide dismutases by the facial nerve transection. Brain Res 582:342–345.

Yu WHA. 2002. Spatial and temporal correlation of nitric oxide synthase expression with CuZn-superoxide dismutase reduction in motor neurons following axotomy. Ann N Y Acad Sci 962:111–121.

WILEY InterScience® DISCOVER SOMETHING GREAT

Journal of Neuroscience Research 85:2332–2342 (2007)

Hepatocyte Growth Factor Promotes Endogenous Repair and Functional Recovery After Spinal Cord Injury

Kazuya Kitamura,[1,2] Akio Iwanami,[1–3] Masaya Nakamura,[1] Junichi Yamane,[1,2] Kota Watanabe,[1] Yoshinori Suzuki,[4] Daisuke Miyazawa,[4] Shinsuke Shibata,[2] Hiroshi Funakoshi,[4] Shinichi Miyatake,[5] Robert S. Coffin,[6] Toshikazu Nakamura,[4] Yoshiaki Toyama,[1] and Hideyuki Okano[2]*

[1]Department of Orthopaedic Surgery, Keio University School of Medicine, Shinjuku, Tokyo, Japan
[2]Department of Physiology, Keio University School of Medicine, Shinjuku, Tokyo, Japan
[3]Clinical Research Center, National Hospital Organization, Murayama Medical Center, Musashimurayama, Tokyo, Japan
[4]Division of Molecular Regenerative Medicine, Osaka University Graduate School of Medicine, Suita, Osaka, Japan
[5]Department of Neurosurgery, Osaka Medical College, Takatsuki, Osaka, Japan
[6]Department of Molecular Pathology, Windeyer Institute of Medical Science of University College, London, United Kingdom

Many therapeutic interventions using neurotrophic factors or pharmacological agents have focused on secondary degeneration after spinal cord injury (SCI) to reduce damaged areas and promote axonal regeneration and functional recovery. Hepatocyte growth factor (HGF), which was identified as a potent mitogen for mature hepatocytes and a mediator of inflammatory responses to tissue injury, has recently been highlighted as a potent neurotrophic and angiogenic factor in the central nervous system (CNS). In the present study, we revealed that the extent of endogenous HGF up-regulation was less than that of c-Met, an HGF receptor, during the acute phase of SCI and administered exogenous HGF into injured spinal cord using a replication-incompetent herpes simplex virous-1 (HSV-1) vector to determine whether HGF exerts beneficial effects and promotes functional recovery after SCI. This treatment resulted in the significant promotion of neuron and oligodendrocyte survival, angiogenesis, axonal regrowth, and functional recovery after SCI. These results suggest that HGF gene delivery to the injured spinal cord exerts multiple beneficial effects and enhances endogenous repair after SCI. This is the first study to demonstrate the efficacy of HGF for SCI.

Key words: hepatocyte growth factor; spinal cord injury; repair; functional recovery

Spinal cord injury (SCI) is followed by secondary degeneration, which is characterized by progressive tissue necrosis, and many experimental interventions using neurotrophic factors have focused on this posttraumatic inflammatory process to reduce damaged area and promote axonal regeneration throughout the lesion epicenter. Neurotrophins such as nerve growth factor (NGF; Tuszynski et al., 1994, 1996), brain-derived growth factor (BDNF; Jakeman et al., 1998; Vavrek et al., 2006), neurotrophin-3 (NT-3; Grill et al., 1997; McTigue et al., 1998), and glial cell line-derived neurotrophic factor (GDNF; Liu et al., 1999; Blesch and Tuszynski, 2001) have been reported to enhance axonal growth in injured spinal cord, and some of the studies cited above showed that neurotrophins promoted behavioral recovery after SCI (Jakeman et al., 1998; Liu et al., 1999).

Not only neurotrophic support but also angiogenesis after SCI is a critical factor in the endogenous regenerative response to trauma (Casella et al., 2002; Loy et al., 2002). Initial damage to local blood vessels is decisive for the progression of destructive events during secondary degeneration (Mautes et al., 2000) and strategic treatments to improve angiogenesis after SCI showed a relationship between blood flow and functional recovery (Glaser et al., 2004; Guizar-Sahagun et al., 2005). Hepatocyte growth

The first two authors contributed equally to this work.

Contract grant sponsor: Leading Project for the Realization of Regenerative Medicine from the Ministry of Education, Culture, Sports, Science and Technology (MEXT), Japan; Contract grant sponsor: General Insurance Association of Japan; Contract grant sponsor: Terumo Foundation Life Science Foundation (to H.O.); Contract grant sponsor: Grant-in-Aid for the 21st Century COE Program from MEXT (to Keio University); Contract grant sponsor: Keio Gijuku Academic Development Funds.

*Correspondence to: Hideyuki Okano, 35 Shinanomachi, Shinjuku-ku, Tokyo 160-8582, Japan. E-mail: hidokano@sc.itc.keio.ac.jp

Received 1 March 2007; Accepted 26 March 2007

Published online 4 June 2007 in Wiley InterScience (www.interscience.wiley.com). DOI: 10.1002/jnr.21372

factor (HGF) was first identified as a potent mitogen for mature hepatocytes (Nakamura et al., 1984; Nakamura et al., 1989) and a natural ligand for the c-Met protooncogene product (Bottaro et al., 1991). Recent studies have revealed that HGF acts as a neurotrophic factor in a variety type of neurons (Hamanoue et al., 1996; Maina and Klein, 1999; Caton et al., 2000) and that HGF administration enhances angiogenesis, improves microcirculation, inhibits the destruction of the blood–brain barrier (Date et al., 2004), and exerts a neurotroprotective effects after cereberal ischemia (Miyazawa et al., 1998; Shimamura et al., 2006). In the present study, we first examined the changes in endogenous HGF and c-Met expression after rat SCI and then determined whether the administration of exogenous HGF into the injured spinal cord using HSV-1 vector had positive effects on histological changes and the motor function after SCI. To the best of our knowledge, this is the first study to examine the efficacy of HGF for SCI.

MATERIALS AND METHODS

Administration of HGF by HSV-1 Vector and SCI

Adult female Sprague-Dawley rats (230–250 g; Clea, Tokyo, Japan) were used for all the experimental groups. All animals were handled in accordance with the Laboratory Animal Welfare Act, the *Guide for the care and use of laboratory animals* (National Institutes of Health), and the guidelines and policies for animal surgery provided by the Animal Study Committee of the Central Institute for Experimental Animals of Keio University. Rreplication-incompetent HSV-1 vectors, HSV-HGF and HSV-LacZ, were obtained as described by Zhao et al. (2006). Rats were anesthetized, their spinal cords were exposed by laminectomy at T10, and 10 μl of HSV-HGF or HSV-LacZ (each titer 1.3×10^9 pfu/ml) was injected into the spinal cord in the HGF group or the LacZ group, respectively (n = 62 each). At 3 days after HSV-1 vector injection, the spinal cords were again exposed at the site of injection, and the region was contused by using the Infinite Horizon impactor (200 kdyn; Precision Systems, Lexington, KY). In the SCI group, contusive SCI was induced at T10 using the IH impactor without the prior injection of HSV-1 vectors (n = 75).

Enzyme-Linked Immunosorbent Assay

Plasma samples were withdrawn transcardially, and a 4-mm-long segment of spinal cord at T10 was isolated and lysed at the indicated times. The spinal cord lysates were prepared with 50 mM Tris-HCl (pH 7.4), 2 M NaCl, 25 mM β-glycerophosphate, 25 mM NaF, 1% Triton X-100, 1 mM phenylmethylsulfonylfluoride (PMSF; Wako, Osaka, Japan), 2 mg/ml antipain (Peptide Institute Inc., Osaka, Japan), 2 mg/ml leupeptin (Peptide Institute Inc.), and 2 mg/ml pepstatin (Peptide Institute Inc.). The concentrations of HGF protein in the extracts of spinal cords lysates and plasma were determined by using ELISA kits (Institute of Immunology, Tokyo, Japan).

Real-Time Quantitative RT-PCR

A 4-mm-long spinal cord segment at T10 was collected at indicated times, and total RNA was isolated from each spinal cord sample using an RNeasy Kit (Qiagen, Bethesda, MD). The levels of HGF and c-Met mRNA were measured as previously described (Sun et al., 2000). The quantitative data for each sample at indicated times was used to determine the ratio relative to that in intact spinal cord.

Immunoblotting Analysis

Lysates from each 4-mm-long spinal cord at T10 were prepared in the same buffer used in an ELISA at indicated times. Proteins (20 μg) were resolved via SDS-PAGE, transferred to a polyvinylidene difluoride membrane, and immunoblotted with a polyclonal antibody (anticleaved caspase-3; 1:500; Cell Signaling Technology, Beverly, MA). Bands were visualized by using an ECL Blotting Analysis System (Amersham Bioscience, Arlington Heights, IL), and the band intensities were measured with an NIH image analyzer. The quantitative data for each band show the relative ratio to that of the spinal cord lysate at 3 days after SCI without any HSV-1 vector injection.

Immunohistochemistry

Spinal cords were perfusion fixed with 4% paraformaldehyde in 0.1 M phosphate-buffered saline (PBS) and postfixed in the same fixative (24 hr), 10% sucrose in 0.1 M PBS (24 hr), and 30% sucrose in 0.1 M PBS (24 hr). Segments of spinal cords were embedded in optimal cutting temperature compound and cut on a cryostat into 20-μm-thick sections. For immunofluoroscence staining, the sections were incubated at 4°C with monoclonal anti-NeuN (1:200; Chemicon, Temecula, CA), monoclonal antiglial fibrillary acidic protein (GFAP; 1:500; Sigma, St. Louis, MO), monoclonal anti-GST-π (1:500; BD Bioscience Pharmingen, San Diego, CA), and polyclonal anti-c-Met (1:50; Santa Cruz Biotechnology, Santa Cruz, CA), followed by Alexa Fluoro-conjugated secondary antibodies (1:500; Molecular Probes, Eugene, OR) and polyclonal anti-rat HGF (1:1; Institute of Immunology) and polyclonal anticleaved caspase-3 (1:400; Cell Signaling), followed by biotinylated secondary antibodies (1:500; Jackson Immunoresearch, West Groove, PA). For diaminobenzidine staining, the sections were incubated at 4°C with polyclonal anti-5-hydroxytryptamine (5-HT; 1:100; Dia Sorin, Stillwater, MN), polyclonal anticholine acetyltransferase (ChAT; 1:50; Chemicon), monoclonal anti-rat endothelial cell antigen-1 (RECA-1; 1:25; Serotec, Raleigh, NC), monoclonal anti-growth-associated protein-43 (GAP-43; 1:2,000; Chemicon), and monoclonal antineurofilament 200 kD (RT97; 1:2,000; Chemicon), followed by biotinylated secondary antibodies (1:500; Jackson Immunoresearch). Biotinylated antibodies were visualized using the Vectastain Elite ABC kit (Vector Laboratories, Burlingame, CA), followed by TSA (Vector Laboratories) or diaminobenzidine (Sigma). All the images were obtained via microscopy (Axioskop 2 Plus; Zeiss, Oberkochen, Germany) or confocal microscopy (LSM510; Zeiss).

Quantitative Analyses

To quantify the RECA-1-positive area and Luxol fast blue (LFB)-stained myelinated area, the images of axial sections were obtained. To quantify the area of the GAP-43-positive fibers and the RT97-positive fibers, the midsagittal sections were scanned and tiled transversely throughout a cephalocaudal

length of 175 μm at the indicated levels of injured spinal cords with a CCD camera (DXC-390; Sony, Tokyo, Japan) using a Micro Computer Imaging Device (MCID; Imaging Research Inc., St. Catharines, Ontario, Canada). The obtained images were analyzed using grain counting with the light intensity by MCID. Threshold values were maintained at constant levels for all analyses. Images of axial sections stained with hematoxylin and eosin were obtained, and manually outlined areas of cavitation were also quantified by MCID. Images of axial sections stained with anti-ChAT antibody and anti-RECA-1 antibody were obtained, and the numbers of ChAT-positive motoneurons in the ventral horns and the numbers of RECA-1-positive vessels with lumina larger than 20 μm were counted.

Behavioral Testing

Motor function of the hindlimbs was evaluated by open-field testing using the methodology of the Basso-Beattie-Bresnahan (BBB) scale at 4, 7, 14, 21, 28, 35, and 42 days after SCI (n = 14 for each group). Throughout the surgery, behavioral testing, and histological analyses, the three researchers who performed the procedures were unaware of the groups to which the rats belonged.

Statistical Analysis

All data are reported as the mean ± SEM. An unpaired two-tailed Student's *t*-test was used for single comparisons. The results of the real-time PCR and ELISA experiments were analyzed via Dunnett test. The Mann-Whitney U-test was used for the BBB score.

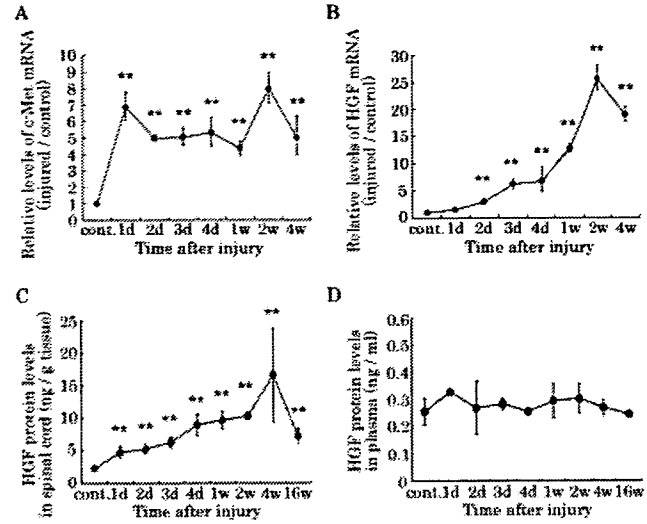

Fig. 1. Endogenous regulation of HGF and c-Met expression after SCI. The levels of c-Met mRNA and HGF mRNA expression after SCI in a 4-mm segment of spinal cord from the lesion epicenter were analyzed by using real-time RT-PCR. In contrast to a drastic increase in c-Met mRNA expression during the acute phase of SCI (**A**), HGF mRNA expression showed a gradual increase only during the subacute phase (**B**). ELISA data show that the amount of HGF protein in a 4-mm segment of spinal cord from the lesion epicenter gradually increased during the subacute phase of SCI (**C**), similar to the pattern of HGF mRNA expression, and the plasma HGF levels did not increase significantly after SCI (**D**). All data were reported as the mean ± SEM. $^{**}P < 0.01$; n > 3 each.

RESULTS

Endogenous Up-Regulation of HGF in Injured Spinal Cord Was Insufficient Compared With the Sharp Increase of c-Met Expression During the Acute Phase of SCI

To determine the dynamics of the HGF-c-Met system in adult rat spinal cord after SCI, the levels of HGF and c-Met mRNA expression in injured spinal cord were analyzed via real-time RT-PCR, and the amounts of HGF protein in injured spinal cord and plasma were also analyzed by an ELISA in the SCI group. Whereas the level of c-Met mRNA expression in injured spinal cord drastically increased from 1 day after SCI (Fig. 1A), the level of HGF mRNA expression gradually increased and peaked at 2 weeks after SCI (Fig. 1B). Thus HGF and c-Met mRNA expression peaked at different time points after SCI. Consistently with the level of HGF mRNA expression, the amount of HGF protein in injured spinal cord gradually increased, peaking at about 4 weeks after SCI (Fig. 1C). In contrast, the amount of HGF protein in the plasma did not increase after SCI (Fig. 1D). Next, we examined the localization of c-Met in normal and injured rat spinal cord. In intact thoracic spinal cord, c-Met immunoreactivity (c-Met-IR) was detected in NeuN-positive neurons and GST-π-positive oligodendrocytes, but not in astrocytes (Fig. 2A–I). However, at 1 week after SCI, c-Met-IR was clearly observed in GFAP-positive reactive astrocytes (Fig. 2J–L; axial section at 5 mm rostral to the epicenter) as well as in neurons and oligodendrocytes (data not shown).

To examine the distribution and amount of HGF protein in uninjured spinal cord after gene delivery, the spinal cord tissues were harvested and processed for an ELISA and HGF immunostaining at 3 days and 4 weeks after the HSV-1 vectors (HSV-HGF and HSV-LacZ) injection. Although HGF-IR showed a remarkable expansion putatively in the extracellular matrix in the HGF group at 3 days after injection, very little HGF-IR was observed in the LacZ group (Fig. 3A). Injection of the HSV-1 vectors resulted in a significantly higher amount of HGF protein in the HGF group (11.5 ± 0.8 ng/g tissue) compared with that in the LacZ group (3.4 ± 0.1 ng/g tissue) at 3 days after injection (Fig. 3C). Double immunostaining using anti-β-galactosidase antibody showed that LacZ gene expression was maintained in NeuN-positive neurons until 4 weeks after the injection (Fig. 3B). There was no significant difference in the amount of HGF protein between the HGF group (4.9 ± 1.5 ng/g tissue) and the LacZ group (2.9 ± 0.1 ng/g tissue) at 4 weeks after the injection (Fig. 3C).

HGF Promotes Survival of Neurons and Oligodendrocytes After SCI

To determine the effects of HGF gene delivery on the injured spinal cord, we performed several quantita-

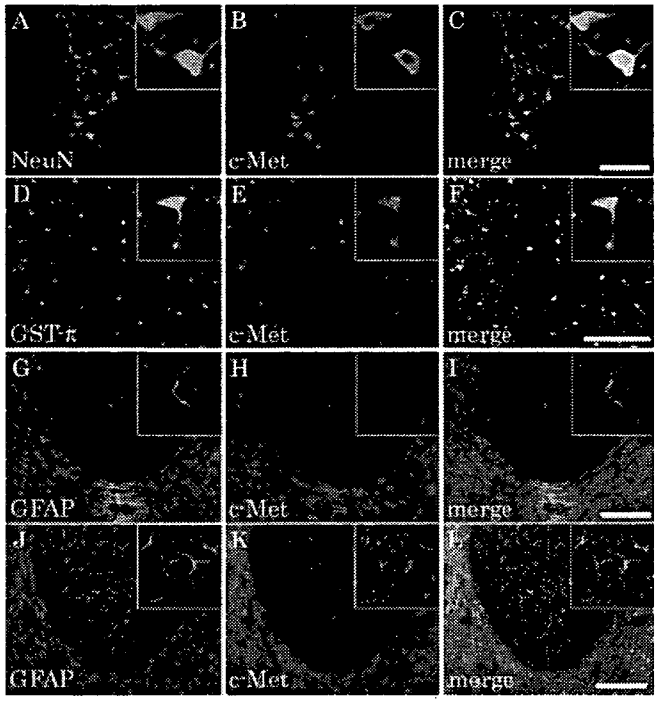

Fig. 2. Change in c-Met immunoreactivity (IR) in neurons, oligodendrocytes and astrocytes before and after SCI. Intact spinal cord showed c-Met-IR in NeuN-positive neurons (**A–C**) and GST-π-positive oligodendrocytes (**D–F**), but not in astrocytes (**G–I**). At 1 week after SCI, c-Met-IR was observed in GFAP-positive reactive astrocytes (**J–L**). **Insets** show magnified view. Scale bars = 200 μm in C (applies to A–C); 100 μm in F (applies to D–F); 200 μm in I (applies to G–I); 200 μm in L (applies to J–L).

tive histological analyses. First, the cavity area of the injured spinal cord at 6 weeks after SCI was obviously smaller in the HGF group than the LacZ group. Significant differences in the total cavity areas at the epicenter and at 4 mm rostral and caudal to the epicenter were observed between the two groups (Fig. 4A). Second, the HGF group obviously had more preserved myelinated areas than the LacZ group at 6 weeks after SCI. Notably, the HGF group exhibited a significantly spared rim of white matter, even at the lesion epicenter, whereas the LacZ group exhibited severely demyelinated white matter throughout the lesion epicenter. Quantitative analysis of the myelinated areas revealed significant differences between the two groups at all of the examined sites (Fig. 4B). Next, to determine the effect of HGF on motoneurons, the numbers of ChAT-positive motoneurons in the ventral horns were quantified at 6 weeks after SCI. Although almost all the ChAT-positive motoneurons had disappeared at the lesion epicenter in both groups, significantly larger numbers of ChAT-positive motoneurons were observed at the site rostral to the epicenter in the HGF group compared with that in the LacZ group (Fig. 4C). These findings suggested that HGF exerted protective effects on motoneurons and oligodendrocytes and contributed to tissue sparing after SCI.

Next, to determine whether HGF inhibited the activation of caspase-3 after SCI, immunoblotting analyses using anti-cleaved caspase-3 antibody were performed at 1, 3, and 7 days after SCI. Cleaved caspase-3 was strongly induced after SCI and was most detectable at 3 days after SCI in both the HGF and the LacZ groups (Fig. 5A). Quantitative analysis revealed that the induction of cleaved caspase-3 was significantly attenuated in the HGF group compared with the LacZ group at 3 days after SCI (Fig. 5B). Furthermore, double immunostaining with anti-cleaved caspase-3 antibody and antibodies for neurons or oligodendrocytes showed that the numbers of NeuN and cleaved caspase-3 double-positive motoneurons in the ventral horns and GST-π and cleaved caspase-3 double-positive oligodendrocytes were

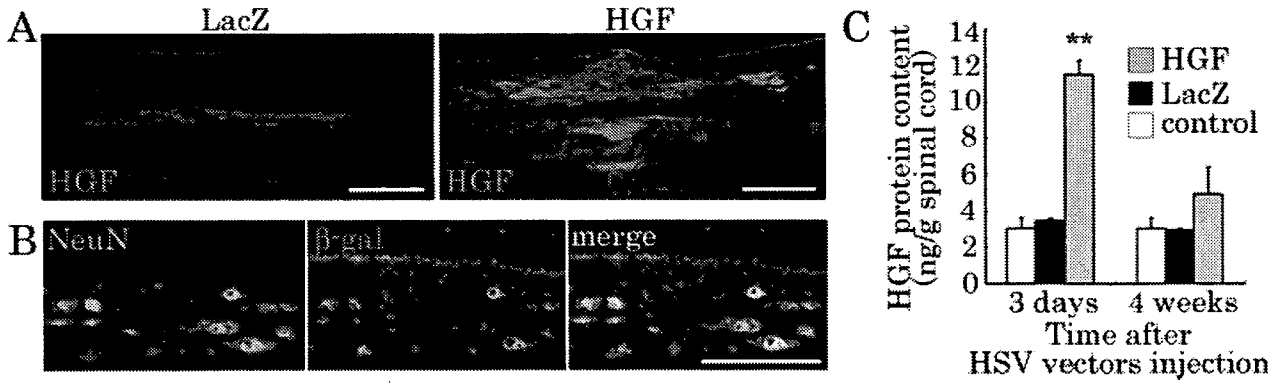

Fig. 3. Expression of exogenous HGF in the spinal cord introduced by HSV-HGF vector. Immunohistochemical staining of rat HGF in sagittal sections at 3 days after the HSV-1 vectors (HSV-HGF and HSV-LacZ) injection into the spinal cords showed remarkable HGF-IR in the extracellular matrix in the HGF group. In all the sagittal sections shown in the present study, the left side is the rostral side (**A**). β-Galactosidase expression was observed in neurons until 4 weeks after the HSV-LacZ injection (**B**). HGF protein levels in 4-mm segments of spinal cords at the site of the HSV-1 vectors injection were analyzed using an ELISA at 3 days and 4 weeks after the injection. The HGF group showed a significantly larger amount of HGF protein than in intact spinal cord (control) and the LacZ group at 3 days after injection. No significant difference in the amount of HGF protein was seen among the three groups at 4 weeks after the injection (**C**). $^{**}P < 0.01$; n = 3 each. Scale bars = 1 mm in A; 100 μm in B.

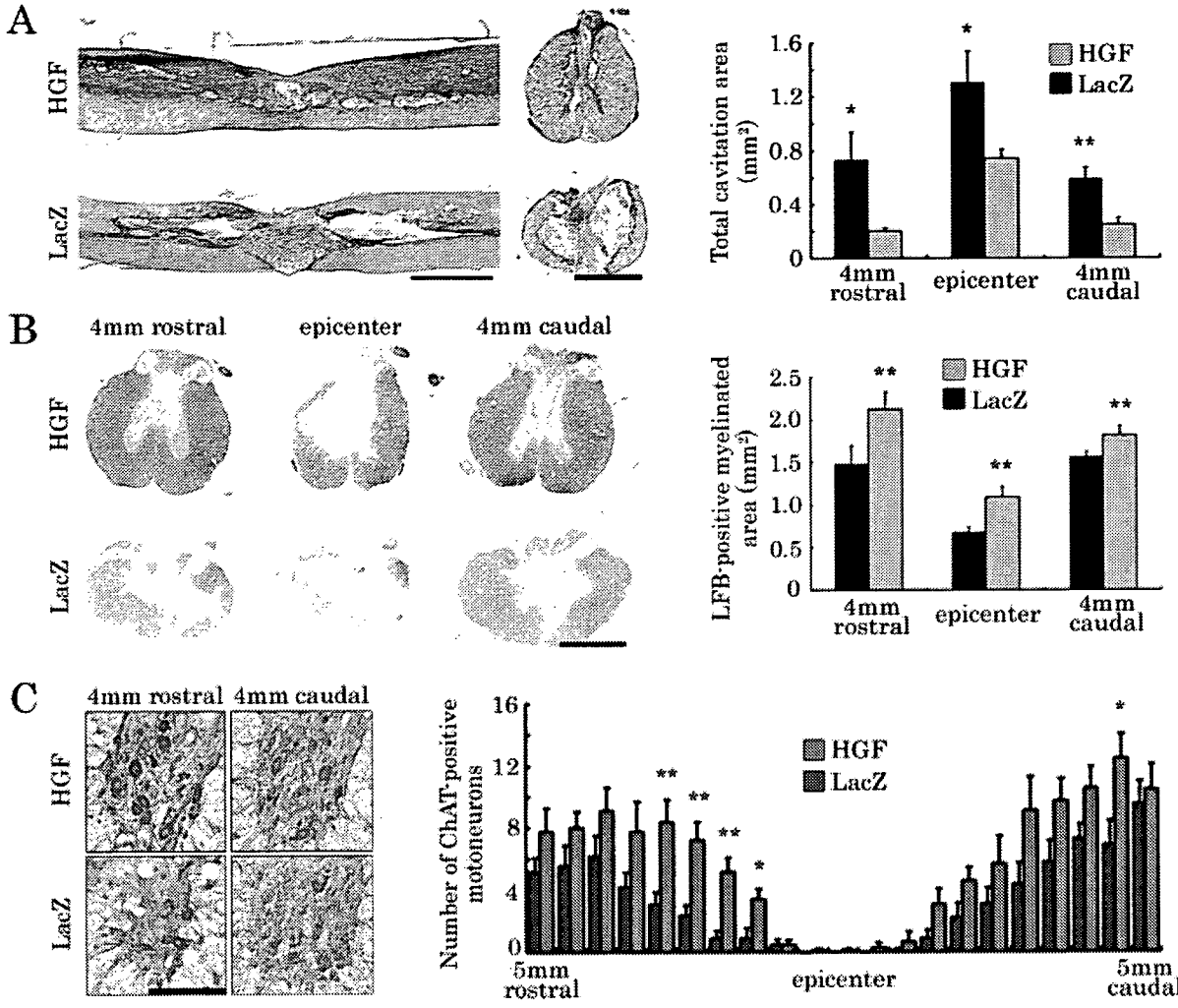

Fig. 4. Significant reduction in the size of damaged parenchyma in the HGF group. HE staining of midsagittal sections and the axial sections of lesion epicenter at 6 weeks after injury showed remarkably smaller areas of damage in the HGF group compared with the LacZ group. Significant differences in the total cavitation areas in the axial sections at the epicenter and at 4 mm rostral and caudal to the epicenter were observed between the two groups (n = 5 each; **A**). The axial sections stained with Luxol fast blue (LFB) at 6 weeks after injury showed a remarkable reduction in the area of demyelination in the HGF group compared with the LacZ group. Quantification of LFB-positive myelinated areas showed significant difference between the two groups at all of the examined sites (n = 5 each; **B**). The number of ChAT-positive motoneurons in the ventral horns at the lesion epicenter and adjacent sections up to 5 mm rostral and caudal to the epicenter in 0.5-mm increments was quantified at 6 weeks after SCI. The pictures show magnified views of right ventral horns of axial sections at 4 mm rostral and caudal to the epicenter. Significant differences between the two groups were observed mainly in the sections rostral to the epicenter (n = 5 each; **C**). $*P < 0.05$, $**P < 0.01$. Scale bars = 2 mm in A left; 1 mm in A right and B; 150 μm in C.

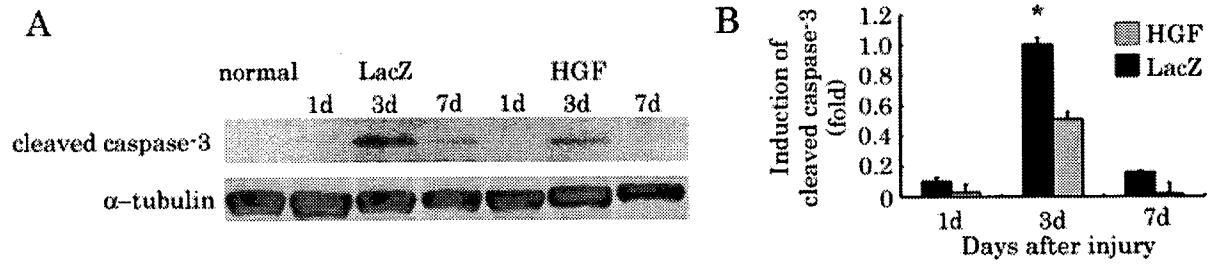

Fig. 5. Induction of cleaved caspase-3 in the injured spinal cord. Immunoblotting analyses showed remarkable induction of cleaved caspase-3 in the HGF and LacZ group during the acute phase of SCI, mainly at 3 days after SCI (**A**). Significantly attenuated cleaved caspase-3 induction was observed in the HGF group, compared with the LacZ group, at 3 days after SCI (n = 3 each; **B**). $*P < 0.05$.

obviously reduced in the HGF group compared with the LacZ group (data not shown). These results suggested that HGF significantly reduced the levels of cleaved caspase-3 activation in neurons and oligodendrocytes after SCI, thereby promoting their survival.

HGF Enhances Angiogenesis After SCI

To examine the effect of HGF on vascular endothelial cells after SCI, immunostaining with anti-RECA-1 antibody was performed. In intact thoracic spinal cord, the vessels had delicate walls composed of homogeneously stained endothelial cells. Although most of the vessels disappeared at the epicenter at 1 week after SCI, several vessels were stained intensely and showed abnormally large lumina with thick walls (Fig. 6A, arrows), which were not observed in the intact spinal cord. Quantitative MCID analysis of the RECA-1-positive areas showed significant differences at the epicenter and 4 mm rostral to the epicenter between the two groups (Fig. 6B). In these areas, there were large amounts of fragmented RECA-1-IR resulting from the debris of dead endothelial cells. Thus, we focused on RECA-1-positive vessels with intact lumina for quantitative analysis. Accordingly, we found that significant differences in the number of RECA-1-positive vessels with lumina larger than 20 μm, representing newly formed vessels (Casella et al., 2002), between the two groups at the epicenter and at 4 mm rostral to the epicenter at 1 week after SCI (Fig. 6C).

HGF Promotes Regrowth of Serotonergic Fibers and Functional Recovery After SCI

To determine the effects of HGF on the axonal growth after SCI, axial sections of injured spinal cords were immunostained with anti-5HT antibody at 1 week and 6 weeks after SCI. 5HT-positive raphe-spinal serotonergic fibers were observed mainly in the gray matter in each group. Quantitative MCID analyses revealed that, whereas 5HT-positive fibers were almost undetectable in either group at 1 week after SCI, a significantly greater abundance of 5HT-positive fibers was detected, even in an area 4 mm caudal to the epicenter, in the HGF group compared with that in the LacZ group (Fig. 7A, arrows) at 6 weeks after SCI (Fig. 7A,B). Furthermore, at 1 week after SCI, the 5HT-positive fibers also showed c-Met-IR (Fig. 7C), and, at 6 weeks after SCI, they expressed GAP-43, which has been used as a marker of axonal regeneration (Kobayashi et al., 1997; Ramon-Cueto et al., 1998; Ikegami et al., 2005; Kaneko et al., 2006), even in a region 4mm caudal to the epicenter (Fig. 7D). Consistently with this, a greater abundance of GAP-43-positive fibers (Fig. 7E,F) and RT97-positive fibers (Fig. 7G,H) was observed, even in a region 4 mm caudal to the epicenter, in the HGF group compared with the LacZ group at 6 weeks after SCI; furthermore, c-Met-IR was also detected in these fibers (Fig. 7I,J). Most of the RT97-positive fibers were oriented longitudinally and parallel to each other (Fig. 7G), and these longitudinal fibers did not express GAP-43 (data not shown), indicating that they probably represented preserved axons after SCI.

The contusive SCI resulted in complete paralysis, followed by gradual recovery, reaching a plateau (BBB score 6.6 ± 1.1) at 6 weeks after SCI in the LacZ group. In the HGF group also, the animals suffered complete paralysis at 1 day after SCI, but these animals eventually showed better functional recovery than those in the LacZ group. Significant differences in the BBB scores were observed between the two groups from 7 days after SCI (Fig. 8). We believe that the difference between a BBB score of 8 (sweeping of hindlimbs) and

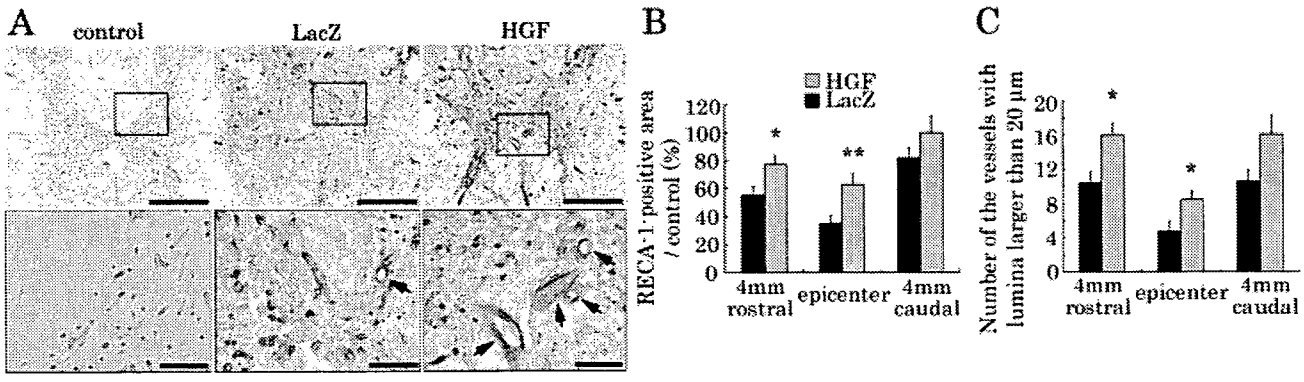

Fig. 6. Change in the microvasculature in the spinal cord after SCI. The axial sections of lesion epicenter at 1 week after SCI and intact thoracic spinal cord were immunostained with anti-RECA-1 antibody (**A**). Higher magnification views correspond to the boxed areas in the upper pictures. RECA-1-positive vessels with abnormally large lumina (arrows) emerged at 1 week after SCI in the two groups; these vessels were not observed in intact spinal cord and were considered to represent newly formed vessels after SCI. Quantitative analysis of the total area of RECA-1-positive endothelial cells (**B**) and the number of vessels with lumina larger than 20 μm (**C**) showed significant differences at the epicenter and at 4 mm rostral to the epicenter between the two groups. $*P < 0.05$, $**P < 0.01$; n = 5 each. Scale bars = 500 μm in A upper; 100 μm in A lower.

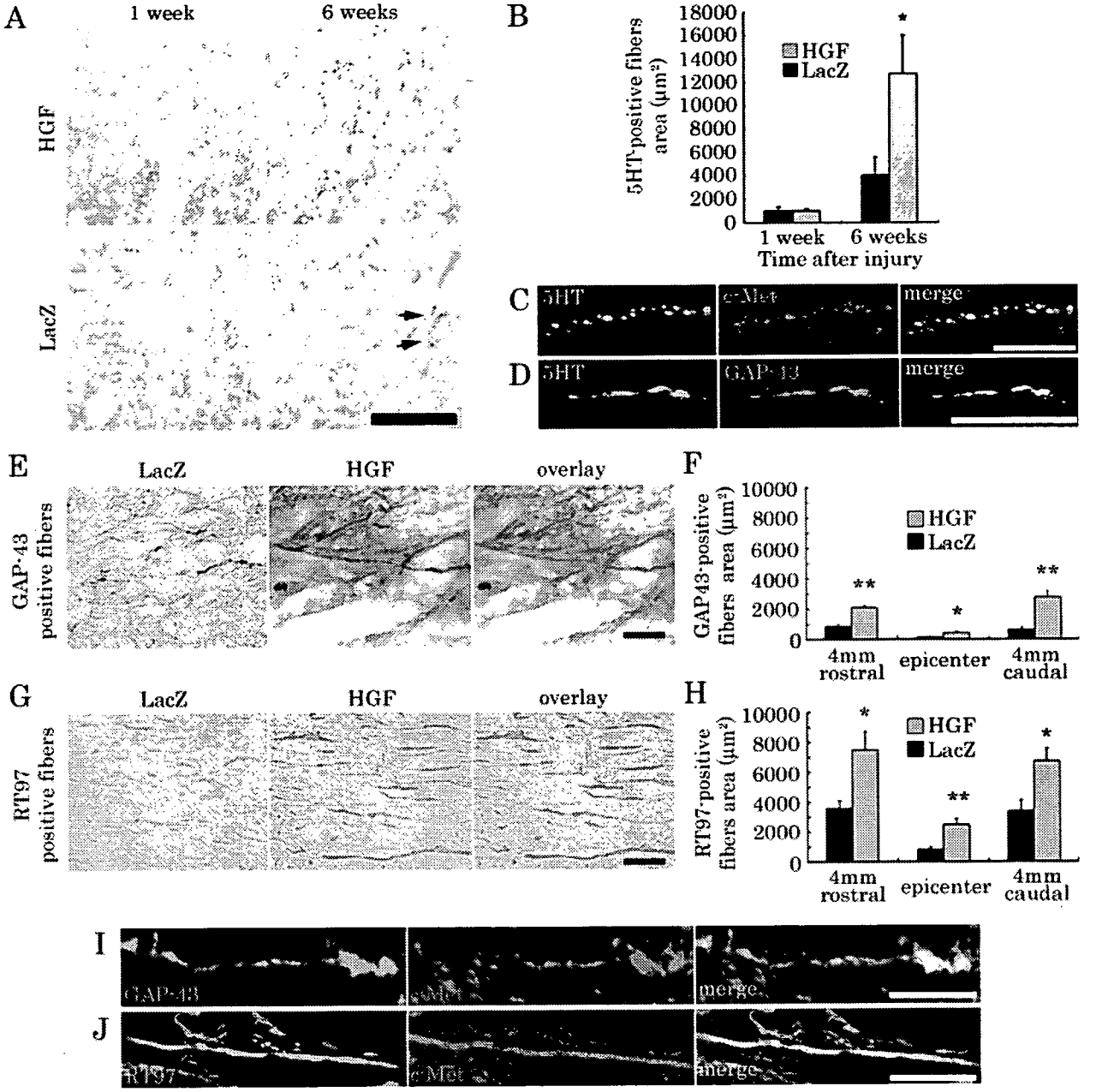

Fig. 7. Degeneration and regrowth of fibers after SCI. Immunostaining and quantification of 5-HT-positive fibers in axial sections at 4 mm caudal to the epicenter showed no significant difference between the two groups at 1 week after SCI but showed significant regrowth of the fibers in the HGF group compared with poor regrowth in the LacZ group (arrows) at 6 weeks after SCI (n = 5 each; **A,B**). 5HT-positive descending raphe-spinal fibers showed c-Met-IR (axial section) at 1 week after SCI (**C**) and expressed GAP-43 (sagittal section) at 4 mm caudal to the epicenter at 6 weeks after SCI (**D**). Representative images of midsagittal sections through an area 4 mm caudal to the epicenter showed a significantly greater abundance of GAP-43-positive fibers (**E**) and R97-positive fibers (**G**) in the HGF group compared with that in the LacZ group at 6 weeks after SCI. Note that significant differences in the immunopositive area were observed even in the region 4 mm caudal to the epicenter between the two groups (n = 5 each; **F,H**). Double immunostaining of midsagittal sections at 1 week after SCI showed c-Met-IR in the GAP-43-positive growth cones (**I**) and RT97-positive neurofilaments (**J**). $*P < 0.05$, $**P < 0.01$. Scale bars = 50 μm in A,E,G,J; 20 μm in C,D; 10 μm in I.

a BBB score of 9 (weight support on hindlimbs) is clinically substantial. From a clinical perspective, the recovery of the HGF group to weight-supported plantar steps (BBB score 10.1 ± 0.6) was noteworthy.

DISCUSSION

Previous studies have shown that the HGF-c-Met system is involved in the mediation of inflammatory responses to tissue injury. In animal models in which the

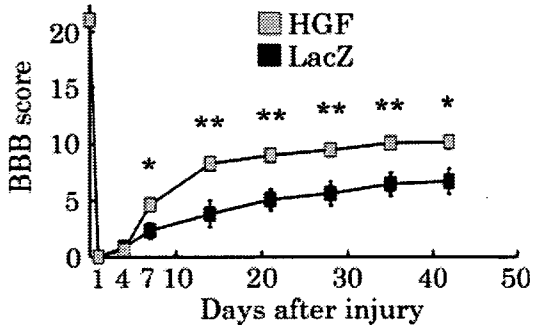

Fig. 8. BBB scores after SCI. A significant improvement in hindlimb motor function was observed in the HGF group compared with the LacZ group from 7 days after SCI (n = 14 each). $*P < 0.05$, $**P < 0.01$.

liver (Noji et al., 1990; Kono et al., 1992; Matsumoto and Nakamura, 1997), lung (Yanagita et al., 1993), or kidney (Kono et al., 1992; Igawa et al., 1993) tissues were experimentally damaged, the HGF mRNA expression and HGF activity were found to increase markedly in the damaged organs, peaking within 24 hr after the insult. Consistently with these increased expressions, the plasma HGF level also increased within 24 hr after the damage, suggesting that HGF could be delivered to these injured organs from other organs through the blood supply via an endocrine mechanism, in addition to being produced endogenously in these organs (Kono et al., 1992). In the CNS, on the other hand, it was reported that HGF mRNA was up-regulated exclusively in the periinfarct region at 14 days after cerebral ischemia (Nagayama et al., 2004). In the present study, we demonstrated for the first time that the HGF mRNA expression level gradually increased, peaking at 2 weeks after SCI, whereas the c-Met mRNA expression level increased markedly within 1 day of SCI. In addition, no increase in the plasma HGF levels was found after SCI. These findings suggest that the injured spinal cord cannot produce a sufficient amount of HGF by itself, compared with the remarkable increase in c-Met expression after SCI, nor can HGF be supplied through an endocrine mechanism, in contrast to the case following damage to other organs, as mentioned above. These results prompted us to perform an in vivo study to determine whether the application of exogenous HGF into the injured spinal cord might exert a beneficial effect and promote functional recovery in the spinal cord after SCI. We used the HSV-1 vector to introduce the exogenous HGF into the spinal cord, to compensate for the deficiency of endogenous HGF after SCI. The feasibility of using this vector for transgene expression in the nervous system in a safe and nontoxic manner has been examined in previous studies (Coffin et al., 1998; Palmer et al., 2000; Lilley et al., 2001).

We showed that the application of exogenous HGF into the injured spinal cord significantly attenuated caspase-3 activation in both neurons and oligodendrocytes, thereby reducing the area of demyelination and promoting the survival of cholinergic neurons. Previous studies have demonstrated the neurotrophic effects of HGF on a variety of neurons (Hamanoue et al., 1996; Maina and Klein, 1999; Caton et al., 2000), and, in one study, the application of HGF prevented the apoptosis of adult motoneurons after axonotomy of the hypoglossal nerve (Okura et al., 1999). In addition, HGF overexpression was reported to prevent delayed neuronal death and decrease the infarct volume after cerebral ischemia (Miyazawa et al., 1998; Hayashi et al., 2001; Shimamura et al., 2004; Niimura et al., 2006) by attenuating apoptosis. Consistently with these reports, in the present study, the neurotrophic and antiapoptotic effects of HGF on the neurons prevented neuronal loss after SCI, thereby reducing the size of the damaged area. Oligodendrocyte death, which is mediated by a pathway involving caspase-11 and caspase-3, leads to demyelination (Hisahara et al., 2001), and inhibition of the apoptosis of oligodendrocytes has been shown to reduce the area of demyelination and functional impairment after SCI (Tamura et al., 2005). These reports indicate that the induction of apoptosis in oligodendrocytes is directly correlated with demyelination and that inhibition of the apoptosis of oligodendrocytes could be potentially beneficial for recovery after SCI. In the present study, we demonstrated that HGF markedly attenuated the induction of caspase-3 in the oligodendrocytes after SCI, resulting in a significant reduction in the area of demyelination after SCI. Taken together, the antiapoptotic and neurotrophic effects of HGF on the neurons and oligodendrocytes contributed to a significant reduction of the area of parenchymal damage after SCI.

HGF is also well known as a potent angiogenic factor. HGF and c-Met are known to be expressed in endothelial cells and vascular smooth muscle cells (VSMCs; Nakamura et al., 1995, 1996), and a relationship between improved microcirculation and behavioral recovery after cerebral ischemia has been suggested (Shimamura et al., 2004, 2006). A change in the microvasculature of the spinal cord after contusion injury has been shown to be essential for the ability of the spinal cord to undergo self-repair (Loy et al., 2002; Hagg and Oudega, 2006). The cordons of vessels that form early at the lesion site may be the initial stage of the trabeculae described in the contusion injury model; these trabeculae have been reported to promote endogenous repair and support axonal outgrowth in the injured spinal cord (Beattie et al., 1997). Loy and colleagues demonstrated a biphasic angiogenic response after SCI, the first phase of which (3–7 days after injury; Casella et al., 2002), but not the second (28–60 days after injury), corresponded to the time course of functional recovery (Loy et al., 2002). Moreover, a relationship between the blood flow and functional recovery has been shown following strategic treatments to improve angiogenesis in the injured spinal cord during the acute phase of SCI (Glaser et al., 2004; Guizar-Sahagun et al., 2005). Thus, enhancing the formation of blood vessels, especially during the acute phase of SCI, may be a potential repair strategy, because nutritional and mechanical support by vessels is critical